Journal of Paleolimnology (2006) 35: 239–270
DOI 10.1007/s10933-005-0096-6

Palaeovariations in the East-Asian monsoon regime geochemically recorded in varved sediments of Lake Sihailongwan (Northeast China, Jilin province). Part 1: Hydrological conditions and dust flux

Georg Schettler[1,*], Qiang Liu[2], Jens Mingram[1] and Jörg F.W. Negendank[1]
[1]*GeoForschungsZentrum Potsdam, Germany;* [2]*Institute of Geology and Geophysics, Chinese Academy of Sciences Beijing, China; *Author for correspondence (e-mail: schet@gfz-potsdam.de)*

Received 22 July 2004; accepted in final form 3 June 2005

Key words: Dust flux, East-Asian monsoon, Geochemistry, Hydrology, Palaeoclimate, Sediments

Abstract

The varved sediments of the dimictic Lake Sihailongwan (Long Gang mountain area, Jilin Province, Northeast China) represent a palaeoclimatic archive which documents the local precipitation frequency during the summer monsoon, and variations in the aeolian flux of dust with their remote sources in the arid and semi-arid regions of inner Asia. Based on a detailed discussion of sediment genesis in Lake SHL, dust flux rates and palaeohydrological conditions were reconstructed on a decadal scale over the past 220 years. The aeolian influx by dry and wet deposition was quantified and characterised in its chemical composition. Photosynthetic production in the lake is positively correlated with the inflow of nutrient-rich groundwater. The groundwater discharge largely reflects the strength of the summer monsoon. Net accumulation rates for biogenic silica were determined for annually laminated sediments from the centre of the U-shaped lake basin based on sediment data. In a Si-balance model of the modern lake, the depositional flux of biogenic silica could be independently quantified on the base of hydrochemical monitoring data. Comparison of the both estimates allowed to asses the focussing of the particle flux in the lake. Though water retention in Lake SHL is rather high (ca. 30 years), changes in the hydrological conditions are sensitively recorded in the sediments because (i) nutrient-rich groundwater discharges into the productive zone of the lake, (ii) a substantial proportion of the total dissolved Si-inventory of the mixed lake (ca. 30%) is annually consumed by diatom growth, and (3) sediment accumulation is substantially focussed towards the flat bottom of the lake basin. The bulk siliciclastic sediment fraction (ca. 75 wt.%) largely originates from influx of dust of remote provenance. In sediment thin-sections, the dry-deposited dust fraction is microscopically identifiable as seasonal silt layer. Aeolian input by wet-deposition shows a distinctly higher variability than the influx of dust by dry-deposition. As diatom production, wet-deposition of dust is positively correlated with the rainfall during the summer monsoon. The inferred positive correlation between rainfall and dust flux during the summer monsoon implies that dust deposition is determined by the out-wash efficiency of mineral particles for a permanent high atmospheric dust concentration over Northeast China in the last 220 years.

Introduction

Atmospheric circulation in East Asia is determined by the interaction of the wind regime, which is forced by the seasonal temperature contrast between the Asian land mass and the subtropical Pacific Ocean with superimposition of the zonal Westerlies, which show a seasonal shift of their

trajectory from ca. 28° N in January to ca. 35° N in July (see, for instance, Xiao et al. 1997), Walker, and tropical Hadley circulation. The strength of the tropical Hadley circulation, which determines the subtropical High in Southeast China, depends on the surface sea water temperature (SST) of the tropical western Pacific which is, in addition to orbital forcing, strongly affected by sea water circulation on a global scale (e.g., Hu 1997). Because of the complex interactions between the above factors, inter-annual variations in the East-Asian monsoon are still unsatisfactorily understood. We expect insights into the variability of the East-Asian monsoon regime by the investigation of annually laminated sediment records from Northeast China.

The weather conditions in Northeast China are strongly influenced by the East-Asian monsoon. They show a distinct contrast between warm and wet weather in summer and severe continental conditions with the prevailing of northwesterly surface wind directions during winter. In the course of the summer, humid air masses from the Pacific push gradually forward in a north-westerly direction into the Asian interior. Mean annual precipitation is contributed in a high proportion by the rainfall during the summer monsoon. Annual precipitation in Northeast China shows a clear decline from southeast to northwest, which is correlated with the gradual progression of the summer monsoon front (Figure 1). The temporal progression and the maximum extension of the summer monsoon front, however, show distinct inter-annual variability, which strongly affects agricultural production in China.

During two field campaigns in the years 1998 and 1999 the crater lakes of the Long Gang mountain area have been investigated for their potential as palaeo-climate archives (Mingram et al. 2004). These investigations lead to the decision to carry out major drilling campaigns in the Lakes Sihailongwan (SHL) and Erlongwan (ERL) in the year 2001 using piston core technique. In a joint German–Chinese research project, a multi-proxy study of sediment records from these lakes, which cover at least the last 60,000 years, has been started.

In this study, we investigate general aspects of sediment genesis in Lake SHL. Based on hydrochemical mass balances, we estimate annual groundwater inflow into the lake and mean evapotranspiration in the catchment of Lake SHL. We elucidate the principle correlation between summer monsoon rainfall, groundwater inflow, and the net accumulation of biogenic opal for Lake SHL and can show that the siliciclastic sediment fraction largely originates from aeolian influx. In detail, we analyse the balance between siliciclastic input of remote and local provenance, the balance between aeolian influx by dry- and wet-deposition, and focussing of the particle flux towards the centre of the lake basin. Groundwater inflow variations are reconstructed on decadal scale.

Lake SHL sediments also represent a natural monitor for palaeovariations in the atmospheric flux of ^{210}Pb. In Part 2 of the study, a detailed reconstruction of the ^{210}Pb flux is given. Derived hydrological variations are validated by the ^{210}Pb flux reconstructions. Estimates for sediment focussing are confirmed in its order of magnitude by the balanced flux of unsupported ^{210}Pb for the centre of the lake bottom (Schettler et al. 2006).

Site of investigation

Lake Sihailongwan (Figures 1b and c), one of a number of crater lakes in the Quaternary Long Gang Volcanic Field (Mingram et al. 2004) is situated in the temperate mixed conifer and deciduous forest region, which roughly extends as a 300–400 km broad band along the most northeastern part of China (Wu 1980). Weather conditions in the Long Gang area are characterised by a distinct seasonal variability, which is determined through the East-Asian monsoon regime. At the nearby meteorological station of Jingyu, mean monthly temperatures are below zero from November to March. In the monitoring period 1955–1997, mean July temperatures varied between 18.8 and 23.5 °C with a mean value of 20.7 °C (Table 1). The summer monsoon front commonly reaches the Long Gang area in early July, which marks the local beginning of the rainy season. Mean annual precipitation of Jingyu is 775 mm. About 85% of annual precipitation falls between May and October (P[MJJASO] = 661 mm). Rainfall during the summer monsoon peaks in July/August and shows distinct inter-annual variability in total amount. Years with enhanced annual precipitation generally have P[JA] values above average. In

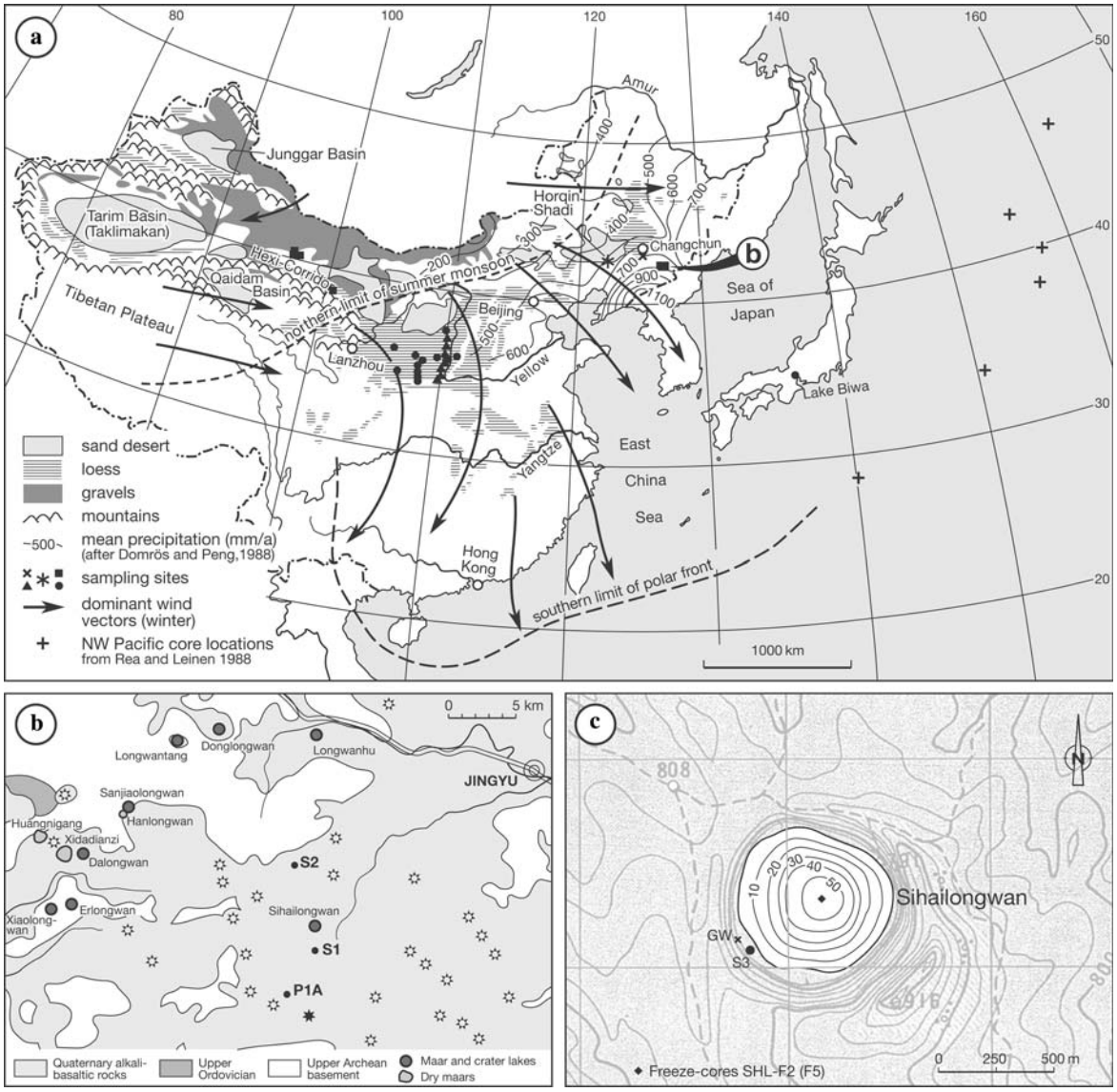

Figure 1. (a) Overview map of East Asia, showing the geographical location of the Long Gang area and probable source regions of the aeolian influx into Lake Sihailongwan. Sampling sites for geochemical data given in Table 4. Filled squares: L-Hexi, Loess (bulk), Ding et al. (2001); filled triangles: LP_m ($< 20\,\mu m$), Sun (2002); *asterisk*: S-TGL, sand dune samples from Horqin Shadi; *cross*: L-CH, non-calcareous loess near Changchun. (b) Map of the Long Gang Volcanic field with major geological units showing the Quaternary volcanic cones and the maar and crater lakes of the region, locations of soil sampling sites are marked. (c) Map of Lake Sihailongwan (SHL) with isobaths and local morphology. Coring sites of the freeze-cores SHL-F2 and SHL-F5, the groundwater sampling site (GW), and soil sampling site S3 are shown.

Jingyu, rainfall of June frequently also was above average for wet years.

Lake Sihailongwan fills a nearly circular U-shaped steeply inclining crater basin. The maximum water depth is 50 m. The crater rim rises up to 121 m above the lake surface at its maximum elevation and is mainly composed of pyroclastic ejecta. Coarse pyroclastic materials deposited within the crater generally favour seepage of rain. The interior of the crater is densely covered by woody vegetation (temperate conifer deciduous forest elements with *Pinus*, *Betula*, *Quercus*, *Ulmus*, *Fraxinus*, *Tilia*, and *Juglans* as the major taxa). The lake does not receive surface inflow by

Table 1. Morphological and hydrological data of Lake SHL.

	Monthly meteorological data					
	Precipitation (mm)		Temperatures (°C)			
	[NDJFMA]	[MJJASO]	[Jan]	[NDJFM]	[July]	[MJJASO]
Mean	114	661	−18.1	−11.0	20.7	14.4
Max.	196	1187	−12.9		23.5	
Min.	56	402	−23.4		18.8	
SD	30	145	2.5		1.0	
Catchment area (m^2)		Elevation (a.s.l.)				
		Lake-surface (m)	Max. crater-rim (m)			
$7.00 \cdot 10^5$		797	918			
Lake						
Diameter (m)	Max. depth (m)	Area (m^2)	Volume (m^3)			
720	50	$4.07 \cdot 10^5$	$9.5 \cdot 10^6$			

Mean total precipitation and data on mean temperatures for the given periods between 1955 and 1997. *Source:* Meteorol. station of Jingyu.

tributaries and has no outlet. There are no signs for significant soil erosion by surface runoff in the interior of the crater.

Coring and sampling

Analytical measurements were undertaken on sediment samples of two freeze-cores recovered from the centre of Lake SHL in 1999 (see Figure 1c for the coring site; for description of the freeze-core system, see Klee and Schmidt 1987). Use of freeze-core technology enabled undisturbed recovery and sub-sampling of the uppermost sediments. Core SHL-F5 was sub-sampled only few days after recovery. It was cut by a handsaw at 1 cm intervals giving 0.8 cm thick sample slices. Core SHL-F2 was sub-sampled in the GFZ-laboratory after return in such a way that the sampling interval closely corresponded with those of the core SHL-F5. The surface of the SHL-F2 freeze-core was prepared and photographed using a stereoscopic binocular microscope. The position of each individual sample was carefully marked on the surface of the freeze-core using the cutting edge of a razor and documented with the photographs taken, so that every sediment sample could be allocated its exact number of annual layers (Figure 2 and Table 2). The individual sample slices were cut exactly along the marks using a diamond saw. The identification of annual laminae involved microscopic thin section investigations using different illumination techniques (incident and transmitted light, dark field). We achieved a close depth correspondence between the individual sediment samples of core SHL-F2 and SHL-F5, which has been confirmed by radiometric measurements (Schettler et al. 2006). Geochemical data presented include a number of loess and soil samples collected during various field campaigns. The geographical location of the sampling sites is shown in Figures 1a–c.

Analytical methods and sample preparation

Sediment samples were freeze-dried and then dry sieved (200 μm) for homogenisation. The remaining coarse fractions accounted for insignificant portions of the total sample dry weights. Water contents were determined by the weight difference before and after freeze-drying. The density of the solid sediment was measured by means of a He-pycnometer (Micromeritics, Accu Pyc 1330). The standard deviation of repeated measurements typically varied between 0.0002 and 0.002 g cm^{-3}. Solid density of sediment samples from the uppermost 3 cm could not be measured with the same high reliability, because of the low amount of available dry substance. Water content determinations of these samples are also of low reliability, since the total amount of ice formed at the sediment/water interface during the operation of the freeze-core equipment obviously exceeded

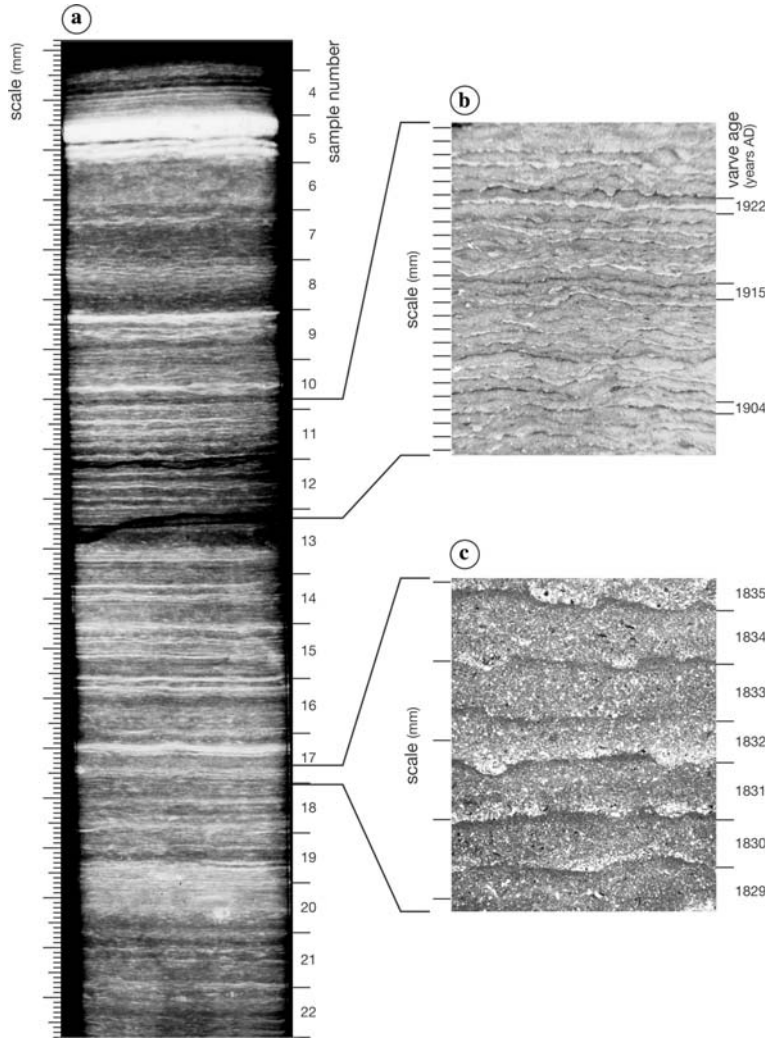

Figure 2. Laminated sediments of Lake Sihailongwan. (a) X-ray image of freeze-core SHL-F2. Seasonal layers with higher contents in siliciclastic matter appear as light bands because of a higher X-ray absorption. The image was taken by the Bundesanstalt für Materialprüfung Berlin. (b) Microscopic surface image, light bands represent seasonal clastic layers, dark laminae show enrichments of organic components. (c) Photograph of a thin section taken with transmitted polarised light showing alternating minerogenic layers (light-coloured) and diatom-rich seasonal laminae (dark coloured).

the real amount of interstitial water in the uppermost sediment section.

For major and trace element analysis, and α-spectrometric determination of ^{210}Po, sample aliquots of 0.25 g dry sediment with addition of a ^{208}Po recovery tracer (Amersham, PMP10020) were decomposed using HNO_3, $HClO_4$, HF in Teflon tubes. The residue was made up to a final volume of 100 ml with HCl. Up to four sample aliquots were digested and unified to a final volume of 100 ml, depending on the expected ^{210}Pb activity (for analytical data see Schettler et al. 2006). Major and trace elements were analysed by ICP-AES (Iris, Thermo Elemental), or ICP-MS (ELAN 5000, Perkin Elmer, see Dulski 2001 for details in ICP-MS measurements) respectively from 1 ml aliquots after further dilution. Total carbon (TC) was analysed by IR-spectrometry after burning aliquots in an oxygen gas flow at 1350 °C, total nitrogen was determined from the same weight aliquots by heat-conductivity detection (LECO, CNS 2000). Inorganic carbon (IC)

Table 2. Sedimentological data and selected flux rates.

Sampl. (number)	Depth (cm)	l [a] (cm)	N_V [a] (yrs)	T_v [a] (yr)	W_c [a] (wt.%)	ρ_s [b] (g cm^{-3})	POR	SR_m (g m^{-2} yr^{-1})	F-bSiO_2 [a] (g m^{-2} yr^{-1})	F-Al_2O_3 [b] (g m^{-2} yr^{-1})
1	0.5	0.50	1.5	1999	98.2(?)	2.2(?)	0.992	91.9		
2	1.5	0.95	3.5	1996.5	96.6(?)	2.2(?)	0.984	94.1		
3	2.5	0.93	6.0	1992.0	92.9(?)	2.280	0.967	115.3		
4	3.5	0.92	6.5	1985.5	85.4	2.367	0.933	225.2	18.0	29.9
5	4.5	0.90	6.0	1979.0	75.5	2.473	0.884	429.4	19.8	66.5
6	5.5	1.05	8.0	1972.0	84.1	2.285	0.924	228.6	25.8	28.3
7	6.5	0.97	9.0	1964.0	84.4	2.259	0.924	184.2	23.8	22.2
8	7.5	0.96	12.0	1953.0	83.4	2.291	0.920	146.3	18.6	18.4
9	8.5	1.00	10.5	1942.0	81.1	2.304	0.908	201.5	22.2	25.7
10	9.5	0.97	12.0	1930.5	81.1	2.336	0.909	171.7	17.5	22.5
11	10.5	1.03	11.0	1919.0	81.6	2.280	0.910	192.1	22.3	25.1
12	11.5	0.96	12.0	1907.5	82.3	2.276	0.914	156.8	17.6	20.7
13	12.5	1.32	16.0	1893.5	77.0	2.307	0.885	218.3	25.5	28.9
14	13.5	1.04	13.0	1879.5	75.7	2.294	0.877	225.8	24.6	30.0
15	14.5	1.03	13.0	1866.0	74.3	2.300	0.869	238.1	27.4	32.2
16	15.5	1.07	17.0	1851.0	75.4	2.270	0.874	179.8	20.9	24.3
17	16.5	1.00	13.0	1836.0	74.8	2.281	0.871	226.1	25.3	30.3
18	17.5	1.02	17.0	1821.0	76.7	2.289	0.883	160.8	20.6	19.2
19	18.5	1.01	15.5	1804.5	75.8	2.289	0.878	182.3	21.9	21.9
20	19.5	1.00	13.5	1790.0	76.4	2.260	0.880	201.6	24.8	22.9
21	20.5	1.10	14.5	1776.0	78.4	2.220	0.890	186.0	25.1	20.8

l – thickness of individual sample slices; N_V – number of varves for the individual sample slices; T_V – dating for the middle of the sample slices; W_c – water content in weight-percent per wet sample; ρ_s – density of the solid sediment; POR – porosity; SR_m – mean annual mass accumulation rate for individual sample slices; F-(…) – balanced flux rates for biogenic silica (SiO_2) and Al_2O_3, respectively.

[a]Based on data of freeze-core SHL-F2.

[b]Based on freeze-core SHL-F5.

was determined coulometrically after the release of CO_2 by reaction with hot phosphoric acid (1:1). Total organic carbon (TOC) was calculated by subtracting IC from TC. Biogenic silica was analysed spectrophotometrically (Mo-blue method) after leaching with 2 M soda solution at 90 °C for 5 h. Before leaching, organic carbon was oxidised using H_2O_2 (30%) and carbonates and authigenic phosphates were removed by treating with hot hydrochloric acid (5%) for 5 min. The remaining siliciclastic residue after leaching with soda was carefully washed with deionised water, and separated from clay-sized particles by repeated centrifugation (1000 min^{-1}, 1 min). Complete separation from clay-sized particles has been checked by Laser-particle analyses for selected samples. The siliclastic sediment fractions, thus derived, consisted of nearly 100% silt ($< 63\,\mu m$). The mineralogical composition of selected silt-samples was determined by XRD-analysis of powdered samples (ca. 1–5 μm) (Stoe Stadi-P diffractometer, Cu $K\alpha_1$ radiation, 2θ-range: 3–125°). The Rietveld program GSAS was used for quantitative analysis (Larson and Von Dreele 1987). The chemical composition of feldspars was estimated on the base of determined lattice parameters.

Soda-leachable silica contents $SiO_2^{(leachable)}$ of 16 soil and loess samples have been determined by the same procedure to estimate possible contributions by leaching of siliciclastic sediment constituents. Leachable SiO_2 of a soil sample from the vicinity of the lake is 1.3 wt.% for the clay-fraction and 1.8 wt.% for the silt fraction (sampling site S3, Figure 1c). Relatively low values of $SiO_2^{(leachable)}$ were obtained for the silt fractions of dune samples from Horqin Shadi (1.0 and 1.1 wt.%). Six calcareous loess samples from the Hexi-Corridor are characterised by slightly higher $SiO_2^{(leachable)}$ contents with higher values for the clay-fraction (2.6–3.6 wt.%) than for the silt (0.9–2.3 wt.%). Loess-like non-calcareous deposits from an uplifted river terrace in Changchun show generally lower values for $SiO_2^{(leachable)}$ (1.5–1.7 wt.%) and the

same values for the clay and silt fractions. Digestion of soil and sediment samples for chemical analyses was carried out under 'normal' pressure conditions. The applied decomposition procedure does not ensure complete dissolution of the mineral zircon. Since heavy rare earth elements (HREEs) commonly show a relative enrichment in this heavy mineral for structural reasons, the calculation of various REE-signatures that are discussed in this manuscript can be affected by incomplete zircon dissolution. We digested a limited number of soil and sediment samples, representing various mineralogical and grain-size compositions, by an alternative decomposition procedure under high-pressure conditions using autoclaves with Teflon-inserts to evaluate probable analytical failures related to incomplete zircon dissolution. According to this assessment incomplete decomposition of zircon did not affect the calculation of Eu_N/Eu_N^* and Ce_N/Ce_N*. Analytical results of normal pressure decomposition, however, gave between 0.15 and 0.3 higher La_N/Yb_N ratios than measurements based on high-pressure decomposition.

Results and discussion

Hydrochemistry and hydrology

Selected hydrochemical data of Lake SHL are compiled in Table 3. Figures 3 and 4 demonstrate the thermal and chemical stratification of the lake for June, September and October; concentrations of Si, Na, and Mg of the local groundwater and rainfall are given inside the diagrams. Dissolved salt concentration (DSC) of the groundwater distinctly exceeds the DSC of the lake water. This reflects a high ratio between precipitation onto the lake surface and inflow of mineralised groundwater. Profiles obtained in mid September 1999 document the dilution of Na and Mg in the epilimnion by the rainfall during the summer monsoon. A slight enrichment of Na and Mg in the surface water is detectable in early summer before the summer monsoon front reached the region.

Total dissolved P concentrations in the local groundwater discharge from 14th September 1999 and from 17th June 2001 were 0.10 and 0.11 mg l^{-1}, respectively. Soluble reactive phosphorus (SRP) in the groundwater sample from June 2001 was 0.083 mg l^{-1}. It is likely that photosynthetic production in Lake SHL is limited by SRP availability during summer stratification (Table 3). However, diatom production may be temporarily limited by Si-availability (Figure 4). After the onset of the rainy season, Si-availability improves in the epilimnion by the inflow of groundwater. Since the lake volume distinctly exceeds the seasonal groundwater inflow and because of substantial dilution by precipitation onto the lake surface, increased inflow of mineralised groundwater is only weakly reflected in the water profiles from the rainy season. In October, when the lake was still thermally stratified and precipitation had declined, inflow of mineralised groundwater became detectable in the epilimnion (Figure 3).

Profiles showing the oxygen isotopic composition in the stratified Lake SHL are presented in Figure 4. The oxygen isotope composition of the local groundwater discharge ($\delta^{18}O_{GW} = -12.2$, 14th Sept. 1999, relative to SMOW-standard, the same for the following), of an individual rainfall event in the rainy season ($\delta^{18}O_{Rain} = -12.3‰$, 21th June 2001), of small rivulets that drain the volcanic area ($\delta^{18}O_{River} = -11.9‰$, 21th June 2001), and of the groundwater discharged into the nearby located Lake Erlongwan ($\delta^{18}O_{GW} = -10.5‰$, 5th July 2001) fall within a range which is in a general good correspondence with published $\delta^{18}O$ data for the mean oxygen isotope composition of the regional precipitation ($\delta^{18}O \approx -10.5‰$, Araguás-Araguás et al. 1998; see also Wei and Gasse 1999; Araguás-Araguás et al. 2000; and the GNIP [Global Net Work of Isotopes in Precipitation] database for Changchun and Haerbin). Lake SHL is characterised by a $\delta^{18}O$ value of $-6.2‰$. The shift towards heavier isotopic composition reflects the isotopic fractionation by evaporation from the lake surface. The order of magnitude in the relative enrichment of ^{18}O (ca. 6‰) implies that the EVP_{Lake}/Inflow ratio is ca. 0.3 (Gonfiantini 1986). For the hydrological data given in Table 1 and assumed mean EVPT of 85% between May and October, such a ratio is achieved with ca. 400 mm annual evaporation from the lake surface. The evaporative effect becomes detectable in the $\delta^{18}O$ profiles of the lake at the beginning of the summer stratification before the onset of the rainy season, direct rainfall

Table 3. Hydrochemical data.

Depth (m)	T^a (°C)	pH[a]	O_2[a] (mg/l)	OSI (%)	Na[b] (mg/l)	K[b] (mg/l)	Ca[b] (mg/l)	Mg[b] (mg/l)	Fe[b] (mg/l)	*c*	*d*	Mn[b] (mg/l)	*c*	*d*	NH_4-N[b] (mg/l)
0	20.9	8.59	8.6	109	2.20	1.44	5.98	2.53	< 0.01	< 0.01	< 0.01	< 0.005	< 0.005	< 0.005	< 0.01
2	21.1	8.57	7.9	92	2.20	1.37	5.98	2.54	< 0.01	< 0.01	< 0.01	< 0.005	< 0.005	< 0.005	< 0.01
4	20.6	8.77	7.6	93	2.19	1.43	5.90	2.50	< 0.01	< 0.01	< 0.01	< 0.005	< 0.005	0.075	< 0.01
6	14.4	8.74	9.8	106	2.17	1.43	5.88	2.49	< 0.01	< 0.01	< 0.01	< 0.005	0.20	0.228	< 0.01
8	10.4	8.57	9.6	95	2.16	1.44	5.87	2.48	< 0.01	< 0.01	< 0.01	< 0.005	< 0.005	< 0.005	< 0.01
10	8.8	8.58	8.8	84	2.17	1.37	5.92	2.50	< 0.01	< 0.01	< 0.01	< 0.005	< 0.005	< 0.005	< 0.01
15	8.5	8.51	5.4	50	2.17	1.42	5.96	2.54	< 0.01	< 0.01	< 0.01	< 0.005	< 0.005	< 0.005	< 0.01
20	8.0	8.36	3.9	35	2.22	1.42	5.95	2.53	< 0.01	< 0.01	< 0.01	< 0.005	0.026	0.106	0.016
25	7.0	7.78	0.5	4.0	2.22	1.43	6.02	2.56	< 0.01	0.051		0.075	0.094		0.036
30	6.2	7.54	0.2	2.0	2.22	1.51	6.07	2.56	0.54	0.47	0.77	0.191	0.143	0.180	0.22
35	5.0	7.11			2.24	1.46	6.24	2.61	1.24	1.09		0.203	0.189		0.33
40	4.5	7.01			2.26	1.45	6.26	2.63	1.64	1.43		0.228	0.209	0.216	0.45
45		6.88			2.24	1.48	6.34	2.64	2.27	1.94	1.65	0.259	0.240		0.54
50					2.24	1.43	6.18	2.60	1.10			0.196			0.32
[b]G.W.					7.63	3.46	11.3	7.74	0.018			0.003			
[c]G.W.					7.27	3.60	12.5	7.90		0.019			0.001		

Depth (m)	F[b] (mg/l)	Cl[b] (mg/l)	SO_4[b] (mg/l)	*c*	*d*	DIC[b] (mg/l)	*c*	*d*	Si[b] (mg/l)	*c*	*d*	P_{total}[b] (mg/l)	*c*	NO_3[b] (mg/l)	SRP[b] (mg/l)
0	0.07	0.77	3.8	4.0	4.2	6.5	6.9	6.4	0.03	0.38	0.14	< 0.01	< 0.01	n.d.	
2	0.04	0.75	3.8	3.9	4.2	6.6	6.6	6.1	0.03	0.39	0.15	< 0.01	< 0.01	n.d.	
4	0.07	0.76	4.0	4.0	3.9	6.5	6.5	6.1	0.06	0.39	0.15	< 0.01	< 0.01	n.d.	
6	0.05	0.82	3.6	4.0	3.9	6.5	6.6	6.0	0.12	0.39	0.16	< 0.01	< 0.01	n.d.	
8	0.11	0.71	3.7	3.9	3.9	6.6	7.5	6.1	0.15	0.12	0.16	< 0.01	< 0.01	n.d.	
10	0.03	0.71	3.2	3.8	4.1	6.7	7.4	6.5	0.15	0.09	0.01	< 0.01	< 0.01	n.d.	
15	0.05	0.72	3.6	3.7	3.6	7.3	7.6	6.9	0.32	0.10	0.08	< 0.01	< 0.01	n.d.	
20	0.08	0.87	3.8	3.8	3.7	7.5	7.6	7.3	0.40	0.25	0.42	< 0.01	< 0.01	0.47	
25	0.08	0.75	3.7	3.5		7.8	8.0		0.49	0.40		< 0.01	< 0.01	0.53	
30	0.05	0.77	3.3	3.3	3.1	8.6	8.1	8.2	0.57	0.50	0.55	< 0.01	< 0.01	n.d.	
35	0.07	0.87	3.0	2.7		9.0	8.7		0.69	0.64		0.04	0.029	n.d.	
40	0.06	0.81	2.7	2.5	2.7	9.6	9.2	8.9	0.80	0.73	0.69	0.08	0.049	n.d.	
45	0.08	0.78	2.4	2.3		10.4	9.6	10.0	0.92	0.88		0.02	0.089	n.d.	
50	0.07	0.79	2.8			9.2			0.64						
[b]G.W.	0.08	1.24	6.77			17.5			12.0			0.11		2.9	0.083
[c]G.W.	0.13	1.50	6.36							13.4			0.10		

a: 18th June 2001, 9 a.m.; *b*: 17th June 2001; *c*: 14th Sept. 1999; *d*: 18th Oct. 2001; G.W.: groundwater discharge, sampling site see Figure 1c.

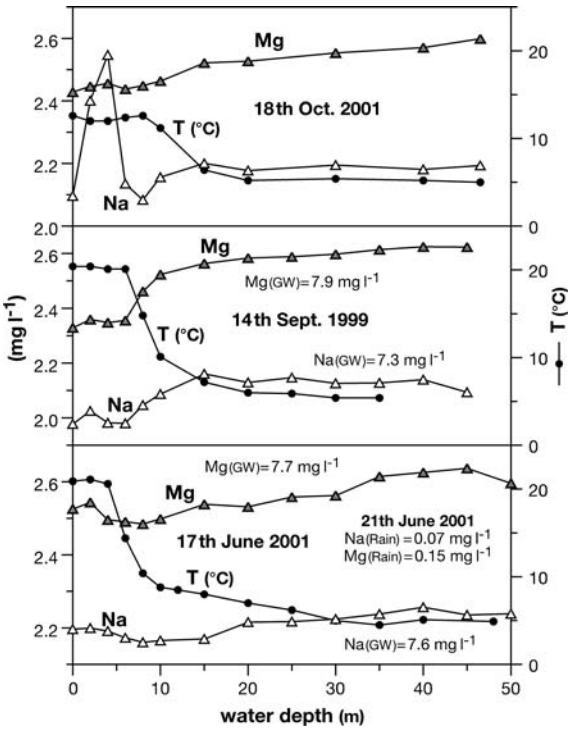

Figure 3. Lake SHL temperature profiles and profiles of Na and Mg from June, September, and October during summer stagnation in Lake SHL. Sampling dates, and Na and Mg concentrations of the local groundwater discharge are shown in the diagrams. Water samples for cation-analyses were membrane filtered (0.45 µm) and stabilised immediately after sampling by adding of HNO_3 (Merck, Suprapur); analysed by ICP-AES (Iris, Thermo Elemental).

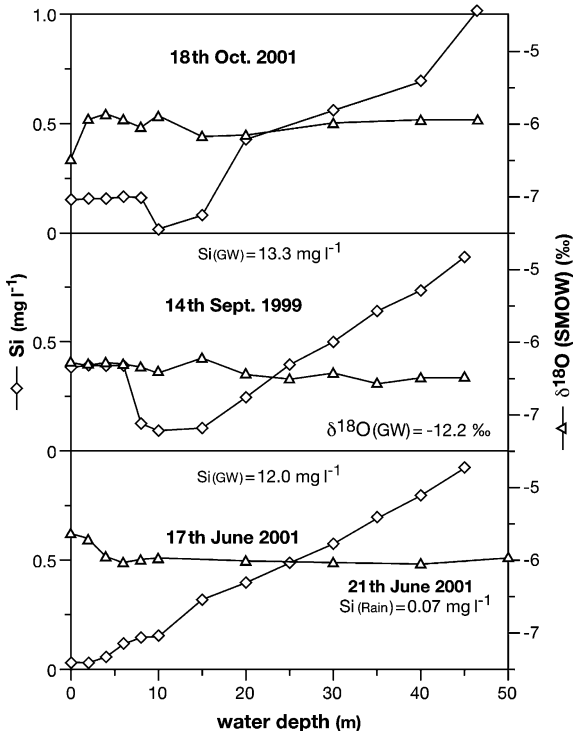

Figure 4. Lake SHL profiles of dissolved silica and $\delta^{18}O$ profiles from June, September, and October. Sampling dates, Si concentrations and $\delta^{18}O$ values of the local groundwater discharge and of local rainfall are shown in the diagrams. Analyst for oxygen isotope data from 2001: Dr B. Mingram (GFZ-Potsdam), data for 1999 measured by Dr A. Lücke (Jülich). The mean $\delta^{18}O$ (SMOW)-value for summer precipitation at the geographical site is −10.5‰ (Araguás-Araguás et al. 1998). The evaporation-effect was detectable in early summer before the summer monsoon front had reached the region. Inflow of groundwater and direct precipitation onto the lake surface becomes detectable at the end of the summer monsoon for declined evaporation (see Figure 5). Determination of Si by ICP-AES (IRIS, Thermo Elemental). Unfiltered water samples were stored in a refrigerator until analyses. Increase of Si in the surface water documents inflow of Si-rich groundwater. The Si-minimum at ca. 10 m depth in September implies enhanced primary production at this depth level. Relative enhanced primary production between 5 and 12 m depth was obvious by the O_2-profile in mid of June 2001 after Si and SRP (soluble reactive phosphorus) had become depleted in the surface water.

onto the lake surface and/or near-surface inflow of groundwater is isotopically detectable in the water profile from October 2001 (Figure 4).

Mass balance calculations of ions, which are only negligibly affected by biochemical cycling, can be used to evaluate the water balance of the lake. Sodium and Mg show low concentrations in local rainfall (Na: 0.07 mg l^{-1}, Mg: 0.15 mg l^{-1}). Input of Na and Mg by inflow of groundwater is diluted to a similar extent by mixing with low-mineralised lake water (Table 3). The concentrations of Na and Mg in the modern lake represent equilibrium concentrations that have been adjusted over a long period. Figures 5a–c show the asymptotic increase of Na and Mg in a hypothetical lake with initial Na(Mg) concentrations of 1 mg l^{-1} for various values of EVPT, if formation of groundwater only by seepage of rain during the summer monsoon (MJJASO) is considered. The balanced Na(Mg)-equilibrium concentrations fit the Na and Mg contents of the modern lake for an EVPT-value of ca. 85%. This value is a plausible estimate of EVPT for the dense woody vegetation in the catchment of the lake. The decrease of Na

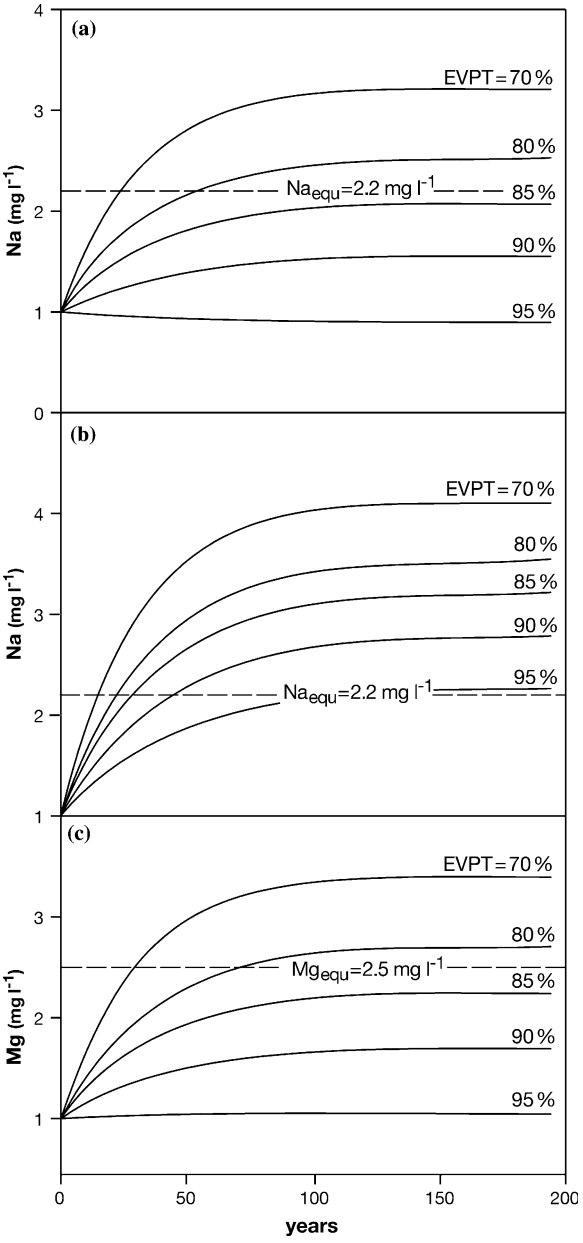

Figure 5. Adjustment of Na equilibrium concentrations within the mixed Lake SHL. (a) Adjustment of Na_{equ} for various values of evapotranspiration (EVPT) during MJJASO. Hydrochemical data: $Na_{(initial)}$ = 1 mg l^{-1}, $Na_{(Rain)}$ = 0.07 mg l^{-1}, $Na_{(GW)}$ = 7.5 mg l^{-1}. Precipitation P[MJJASO] = 661 mm, P[NDJFMA] = 114 mm, no percolation of winter precipitation, EVPT [NDJFMA] = 50%, evaporation from the lake-surface EVP_{Lake} = 400 mm, $V_{Lake} = 9.5 \cdot 10^6$ m^3, $A_{Lake} = 4.07 \cdot 10^5$ m^2, $A_{Catchment} = 7.0 \cdot 10^5$ m^2. (b) Same conditions as in (a), but 50% percolation of winter precipitation taken into account. (c) Adjustment of Mg equilibrium concentrations within the mixed Lake SHL for various values of EVPT during MJJASO, same hydrological data as in (a), $Mg_{(initial)}$ = 1 mg l^{-1}, $Mg_{(Rain)}$ = 0.15 mg l^{-1}, $Mg_{(GW)}$ = 7.8 mg l^{-1}.

and Mg for the upper 5 m of the water column by ca. 0.2 mg l^{-1} in September '99 (Figure 3) can be obtained in this order of magnitude by dilution through rainfall onto the lake surface during July, August, and September. Assumed significant contributions to the groundwater discharge by winter precipitation (half of total precipitation during NDJFMA) do not fit the Na concentration of the modern mixed-lake (Figure 5b) and are therefore unlikely.

Sediment structure and varve chronology

The sediments of Lake SHL show seasonal laminations (see Figure 2). Typically, a 50–200 µm thick diatomaceous layer, mainly attributed to *Cyclotella* cf. *Radiosa* and *Cyclotella* cf. *Pseudostelligera* is overlain by a 50–200 µm thick clastic layer with silt-sized debris as the major constituent. Since *Pinus* pollen occurs frequently above this layer, enhanced siliciclastic influx is probably related to spring (Mingram et al. 2004). Monthly sediment trap data from Lake SHL support this interpretation. The absolute highest depositional flux of minerogenic matter above the flat lake bottom was recorded in a sediment trap, which was exposed immediately after the lake had become ice-free on 14th of April 2002 (Chu et al. 2005). Thin section investigations reveal a mixed layer of autochthonous biogenic components, terrestrial plant debris, and minerogenic particles following the siliciclastic layer (Mingram et al. 2004). The monthly sediment trap data document three seasonal diatom blooms in May, September, and November for the period 2002–2003. Enhanced deposition of diatomaceous matter is hard to identify in thin sections because of the high minerogenic background. The very thin, but distinct diatom layer between the mixed layer and the siliciclastic spring layer could be settled during the winter stagnation from the autumn bloom and/or results of an early spring diatom bloom under the ice cover of Lake SHL. However, the seasonal sediment structure of the SHL-sediments clearly allowed identifying of annual laminations (varves). The accuracy of varve counting for the last 200 years is about 1–2%. The numbers of varves counted for each individual sample are given together with sedimentological data in Table 2.

Physical, mineralogical, and chemical sediment characteristics

The variation of porosity and water content in the upper sediment sequence reflect the early diagenetic compaction of the sediments (Table 2). With the exception of sample 5, which includes several thick clastic layers (see Figure 2a), and the adjoining sample 4, the dry density of the solid sediment (ρ_s) varies within a close range (2.220–2.336 g cm^{-3}). The mass accumulation rate (SR_m) shows a distinct maximum for sample 5.

The major mineral constituents in the silt fractions of samples 5 and 12 as analysed by XRD are quartz (58 and 56 wt.%), albite (24 and 23 wt.%), orthoclase (7 and 3 wt.%), and a basic plagioclase (4 and 7 wt.%; $\sim ab_{20}an_{80}$) which account together for 90 wt.% of the bulk silt. There are minor contributions from hornblende and clay minerals (vermiculite, chlorite, kaolinite). The balance between the major mineral constituents in these samples corresponds with Al_2O_3 concentrations of 7.8 and 8.5 wt.% for the bulk silt, which is a minimum estimate since pumic tuff (variation range of 19 local alkalibasalts: 14–16 wt.% Al_2O_3, Schettler, unpublished data) and Al_2O_3-rich clay minerals are not considered in this balance.

Selected geochemical data of the uppermost 27 cm sediment (ca. 320 years, Mingram et al. 2004) are shown in Figure 6. The non-calcareous sediments (IC < 0.01 wt.%) are composed of clay- to silt-sized mineral particles (Al_2O_3: 10.1–15.5 wt.%) and biogenic components (biogenic silica: $bSiO_2$ = 4.6–16.1 wt.%, TOC: 4.4–17.3 wt.%). Leaching of SiO_2 from the siliciclastic sediment constituents may overestimate the biogenic silica content that originates from autochthonous production by a maximum value of 1 wt.% (see Section 'Analytical methods and sample preparation'). TOC/N (mole/mole) shows a continuous decrease from 15 to 10 between 27 cm and the top of the sediment. A distinct increase of TOC and S^{total} above 5 cm documents enhanced deposition of organic matter together with reduced aerobic mineralization of the organic deposit (Figure 6). From the increase of S^{total}/TOC, it can be concluded that the diffusive flux of sulphur (sulphate) across the water/sediment interface increased synchronously. This may well depict longer periods of oxygen depletion in the bottom water of the lake as well as a probable increased SO_4^{2-} lake water concentration which is ca. 4 mg l^{-1} in the surface water of the recent lake (Table 3). A plausible estimate for the 'light' total autochthonous sediment fraction (Au^{total}) is given by '($bSiO_2$)·2.2' below 9 cm and by '($bSiO_2$)·2.5' for sediments above 9 cm which are affected by eutrophication (see Appendix A for detailed explanations). The total allochthonous siliciclastic sediment fraction (All^{total}) is balanced by (Al_2O_3)·100/17.5. Estimates of All^{total} by (100 − Au^{total}) give confirming results (Figure 7) and typically accounts for 75 wt.% in the balanced sediment section.

A major portion of the siliciclastic influx is of remote origin (see following Section 'Balance between siliciclastic input of local and remote origin'). The local alkali-basalts and the SHL sediments show major differences in some of their geochemical signatures (Table 4). The SHL sediments, for instance, have higher Al/Ti, Al/Mg, and La/Yb values than the pyroclastic debris. The Co/Al and Rb/Cs values of the lake sediments are distinctly lower than the range for the alkali-basalts. The PAAS-normalised REE-concentrations of the SHL-sediments and of the local Quaternary pumic tuffs are geochemically characterised by a positive Eu-anomaly (see Appendix A for explanation of used abbreviations), which is distinctly higher for the alkali-basaltic rocks (Table 4).

The Pb/Sc ratio increases from ca. 1930 to present (Figure 6). This may have been caused by an increasing atmospheric input of anthropogenic lead, but may also be due to the progressive release of local geogenic lead as a result of the apparent acidification tendency in the watershed area. The obtained Pb/Sc increase is accompanied by a decrease of $^{206}Pb/^{207}Pb$, indicating changing contributions from the previous lead reservoirs, or the input of lead components with lead isotope signatures deviating from the geogenic background of the SHL record (Figure 6). Fe/Al and U/Th, which document variable influx of dissolved Fe and U, distinctly increase in the uppermost sediment section. This confirms increase of weathering in the catchment during the last decades. The increase of U/Th and Fe/Al certainly also documents a general reduction of O_2-availability in the deep water. The net flux of dissolved Fe to the sediments may have increased for enhanced sulphide precipitation and reduced seasonal re-oxidation of these sulphides. The transfer

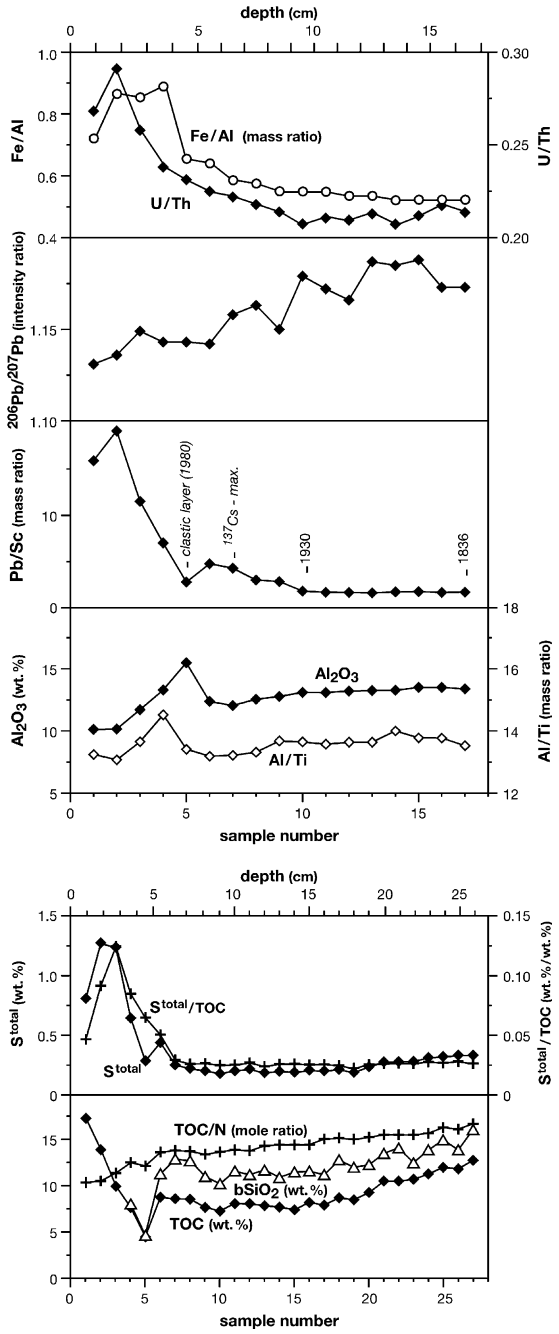

Figure 6. Selected geochemical profiles of Lake SHL sediments. Analytical data based on freeze-core SHL-F2 for biogenic silica ($bSiO_2$), and freeze-core SHL-F5 for the other parameters. Chronostratigraphic data given on the Pb/Sc-profile are based on varve-counting (core SHL-F2) and represent the middle of the individual sample slices.

efficiency of dissolved U is strongly affected by the reduction of U(VI) and scavenging of U(IV) at settling organic matter.

Biogenic silica ($bSiO_2$) is a major constituent of the autochthonous sediment fraction. The concentrations of biogenic silica show a highly correlative trend with TOC (samples 6–27, $R^2 = 0.85$). The TOC/N mole ratio of the SHL sediments (10.4–16.7, Figure 6) is higher than that commonly obtained for algae gyttja (ca. 10). This implies contributions from dissolved or detrital carbon-influx of terrestrial origin. The gradual decrease of TOC/N in younger sediments documents that the deposition of planktonic organic matter has increased during the recent sedimentation history. The concentrations of Al_2O_3 show a corresponding decrease through enhanced dilution. Mean annual mass accumulation rates (SR_m) and calculated net accumulation rates for biogenic silica (F-$bSiO_2$) are compiled in Table 2. The derived flux rates of biogenic silica reflect variations in the primary production of the lake. The highly correlative trend between F-TOC and F-$bSiO_2$ (Figure 8) implies that variations in the accumulation of the autochthonous sediment fraction largely reflect variable deposition of planktonic matter. The SHL sedimentation record, however, does not show a related decrease in TOC/N for enhanced deposition of biogenic silica or planktonic matter, respectively (Figure 9). The input of terrestrial organic carbon originating from dissolved or detrital influx from the vicinity of the lake and/or from aeolian deposition of plant remains of remote provenance clearly shows variability paralleling the bio-productivity of the lake.

The derived flux rates for Al_2O_3, which document variations in the influx of aluminosilicates, are positively correlated with F-TOC ($R^2 = 0.92$) and F-$bSiO_2$ ($R^2 = 0.95$), respectively (Figures 10 and 11). Wet scavenging efficiently removes fine mineral aerosols from the atmosphere. Recent studies (Wilcox and Ramanathan 2004, and references therein) demonstrate the close correlation between rainfall frequency and dust deposition for Asia and how the rainfall belt of the intertropical convergence zone (ITCZ) efficiently prevents transport of dust by north-easterly monsoon winds towards the Southern Hemisphere. If the derived F-Al_2O_3 variability would reflect changes in summer monsoon rainfall over Northeast Asia, F-TOC and F-$bSiO_2$ might be also seen as proxies for the summer monsoon strength.

Sedimentation during the last few decades is characterised by a relative increase in the

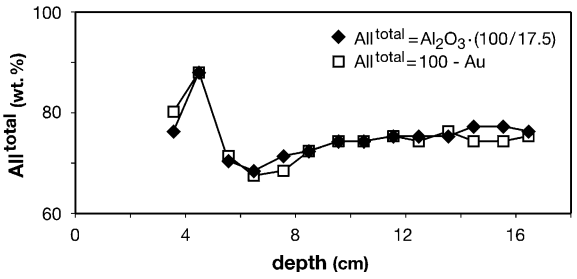

Figure 7. Various estimates for the bulk siliciclastic sediment fraction (All^{total}), based on the concentrations of Al_2O_3 and estimates for the bulk autochthonous sediment fraction (Au^{total}), respectively. Filled diamonds: $All^{total} = Al_2O_3 \cdot (100/17.5)$, open squares: $All^{total} = 100 - Au^{total}$, $Au^{total} = bSiO_2 \cdot x$, x = 2.2 for sediments below 9 cm and x = 2.5 for sediments above, see Appendix A for further explanations.

deposition of autochthonous components. In the F-TOC–F-Al_2O_3 and F-bSiO_2–F-Al_2O_3 diagram, respectively, the samples 6, 7, and 8, which document this change in sedimentation between 1950 and 1970, therefore plot below the trend lines defined by older samples (samples 9–17, 1830–1947). Enhanced input of siliciclastic material at 4.5 cm (sample 5, Figure 2) is not attributed to local soil particles washed in from the interior of the crater but rather to aeolian fall-out during dust storms. Sample 5 (ca. 1980) reveals no geochemical signatures indicative of an increased input of local volcanic material. Increased minerogenic detritus concentration within a corresponding time-horizon and supporting our interpretation, was found in the sediment record of another lake in the Long Gang area (Lake Sanjiaolongwan, Schettler et al. 2006). Particularly conspicuous is the deposition of sediments with high Al/Ti ratio in sample 4 (Figure 6) after the enhanced minerogenic input for the period represented by sample 4. This seems to reflect enhanced deposition of clay-sized particles in the centre of the lake basin over a period of several years following the increased dust fall-out.

Forcing of biogenic autochthonous deposition

Primary production in lakes depends on temperature, light and nutrient availability. These parameters show distinct seasonality for Lake SHL. The balanced net accumulation rates of TOC and biogenic silica of individual sediment samples represent mean values for periods between 6 and 17 years (Table 2). On this time scale, they should largely document changes of nutrient availability in the phototrophic zone of the lake. Hydrochemical profiles of Lake SHL, taken during summer stratification, imply limitation of primary production by P and Si availability (see Section 'Hydrochemistry and hydrology', Table 3, Figure 4).

External forcing of photosynthetic production

The lake does not receive influx of nutrients by tributaries and there are no signs for significant surface run-off from the vicinity of the lake. In such a type of lake, groundwater inflow commonly represents the major nutrient source for phytoplankton (Hurley et al. 1985). This correlationship is confirmed for Lake SHL by hydrochemical data (Table 3). The Si concentration, measured in the local groundwater discharge, exceeds that of the mixed lake about 30-fold, total P accounts for 0.1 mg l^{-1} in local groundwater. The low dissolved Si concentration of local precipitation, measured during a single rainfall event (0.07 mg l^{-1}), is insignificant for the Si-balance of the lake; dissolved P was not detectable in the rain.

Dissolved influx of algae nutrients via groundwater inflow is sustained by the decay of organic matter, and by chemical alteration of siliciclastic materials deposited in the catchment of the lake. Algae nutrients are continuously released by silicate weathering and decay of organics for the warm and humid conditions that prevail during summer. Particularly, weathering of the alkalibasaltic pumic tuff may highly contribute to the dissolved influx of P and Si.

The variability in annual precipitation (SD = 149 mm) is largely related to precipitation during the summer monsoon which accounts for ca. 85% of annual precipitation (Table 1). Furthermore, there is no possibility for percolation of precipitation between November and March when the topsoil is frozen. Rainfall during the summer monsoon and groundwater inflow from the small catchment of the lake therefore should be positively correlated.

The low salt concentrations in Lake SHL (Table 3) reflect that inflow of mineralised groundwater is much lower than direct precipitation onto the lake surface. The interior of the SHL crater is densely covered by mixed deciduous/coniferous woody

Table 4. Selected geochemical signatures of SHL-sediments and probable input components.

	Local ign. rocks	SHL-sediments				Local soils						Remote components						
	1	2				3						4	4	5	6	6	7	7
	Alkalib.[a] (m), $n = 7$	T1[a]	$F5_m$(9–17)	F5(5)	F5(4)	$F5_{dry}$[c], $n = 4$	$F5_{wet}$[c], $n = 6$	S2 clay, $n = 7$	S2 silt, $n = 7$	S3 clay, $n = 1$	S3 silt, $n = 1$	P1A, 4–44, $n = 19$	P1A, 44–69, $n = 14$	L-Ch clay, $n = 5$	L-Ch silt, $n = 5$	S-TGL silt, $n = 5$	LP_m, $< 20\,\mu m$, $n = 11$	Loess bulk, $n = 7$	L-Hexi clay, $n = 40$	L-Hexi silt, $n = 40$
Al_2O_3	16.0	16.4	13.2	15.5	13.3	13.1	13.2	17.6	14.5	18.2	13.3	14.1	15.5	19.1	11.4	11.1			16.8	11.7
Th/U	4.9	5.0	4.7	4.3	4.2	4.7	4.7	5.2	4.7	4.8	4.6	4.7	4.3	4.0	4.2	5.3	5.2	4.1	3.7	4.2
Major contrast to local alkali-basalts																				
Mg/Al	0.53 (0.06)	0.42	0.130 (0.002)	0.111	0.121	0.131 (0.003)	0.129 (0.002)	0.119 (0.02)	0.25 (0.09)	0.111	0.144	0.098 (0.002)	0.130 (0.015)	0.108 (0.01)	0.069 (0.006)	0.067 (0.005)			0.35 (0.02)	0.33 (0.01)
Co/Al	5.2 (0.6)	4.3	2.3 (0.1)	3.4	4.1	2.4 (0.07)	3.3 (0.2)	3.3 (0.2)	3.6 (0.6)	2.8	2.40	2.1 (0.5)	4.7 (0.7)	1.4 (0.4)	1.9 (0.6)	0.84 (0.05)			2.5 (0.12)	2.0 (0.11)
Eu/Eu*	1.93 (0.06)		1.33 (0.02)	1.28	1.32	1.34 (0.02)	1.32 (0.01)	1.56 (0.06)	1.56 (0.08)	1.42	1.41	1.29 (0.03)	1.42 (0.03)	1.15 (0.01)	1.21 (0.02)	1.22 (0.04)	1.18 (0.01)	1.19	1.15 (0.03)	1.17 (0.02)
Strongly depending on grain size composition																				
Al/Ti	5.8 (0.3)	5.6	13.7 (0.14)	13.4	14.5	13.6 (0.17)	13.7 (0.16)	8.4 (0.8)	9.3 (0.7)	8.8	9.6	11.5 (0.7)	9.9 (0.5)	21.7 (0.8)	12.9 (0.6)	15.4 (0.9)			20.3 (0.5)	13.7 (0.8)
Divergent petrochemical trend for local alkali-basalts																				
La_N/Yb_N	0.5–2.2	1.72	1.15[b] *A1u10–12*	1.32	1.30	1.29 (0.03)	1.28 (0.03)	1.54[b] *S2-C*	1.37[b] *S2-C*	1.44	1.46	1.18[b] *P1A(10–12cm)*		1.12[b] *L-ChE*	0.87[b] *L-ChE*	0.82[b] *TGL-1*	0.945 (0.04)	0.83	0.95[b] Hexi S3–S5	0.94[b] Hexi S3–S5
Strongly affected by exogenic reactions																				
Ce/Ce*	0.94 (0.01)	0.96	0.93 (0.01)	0.95	0.96	0.93 (0.01)	0.93 (0.01)	1.13 (0.15)	0.99 (0.12)	1.16	0.98	1.05 (0.04)	1.08 (0.06)	0.73 (0.16)	0.94 (0.09)	0.95 (0.01)	0.950 (0.01)	0.96	1.00 (0.02)	1.00 (0.01)
Rb/Cs	67–113	93	14.7 (0.2)	14.4	15.2	14.7 (0.10)	14.8 (0.25)	13.5 (1.6)	18.1 (2.8)			15.6 (1.0)	15.3 (0.7)	10.9 (0.4)	20.4 (2.0)	28.0 (1.3)			11.1 (0.5)	16.3 (1.0)
K/Na	0.43–0.67	0.6	1.69 (0.06)	1.60	1.49	1.67 (0.09)	1.67 (0.05)	1.9 (0.4)	0.91 (0.08)	4.0	1.0	1.53 (0.1)	1.49 (0.1)	21.5 (4.5)	1.9 (0.3)	1.2 (0.06)			4.3 (0.3)	1.3 (0.09)
Zn/Al	10.1 (0.7)	9.3	14.0 (0.5)	14.0	19.7	14.9 (1.0)	14.2 (0.5)	13.4 (1.7)	10.6 (1.4)	14.1	9.0	11.5 (0.9)	11.3 (0.5)	9.5 (0.3)	6.5 (0.4)	5.5 (0.5)			15.8 (0.6)	11.3 (0.4)

1: Mean chemical composition of alkali-basaltic lava (B1) and pumic tuffs (T) from the Long Gang Volcanic Field (ERL-, ERL-T1, SHL-B1, XIA-T_{black}, XIA-T_{red}, SHL-Soil-T1. SHL-Sed-T1, the first capital letters give the sampling location: (ERL = Lake Erlongwan, SHL = Sihailongwan, XIA = Xiaolongwan, see Figure 1b). T1: 7.5 cm thick pumic tuff layer occuring in the SHL sedimentation record between 108 and 115.5 cm depth.

2: SHL-sediments between 3 and 17 cm depth, freeze-core SHL-F5, $F5_m$ mean values for samples 9–17, F5(5) clastic layer, F5(4) adjoining section with distinct enhanced Al/Ti, $F5_{dry}$ mean values for dry periods (sample 8, 10, 12, 16), and $F5_{wet}$ for wet periods (samples 9, 11, 13–15, 17), see Figure 9.

3: Grain size fractions of soil samples from the Long Gang area, sampling locations are shown in Figure 1b.

4: Mean of non-calcareous loess samples from Changchun, $< 2\,\mu m$ and 2–63 μm fractions, sampling location shown in Figure 1a.

5: Mean of silt fractions of non-calcareous sand dune samples from Horqin Shadi.

6: Loess from the Loess Plateau, LP_m ($< 20\,\mu m$): Mean of the $< 20\,\mu m$ fractions, sample information and sampling locations given in Sun (2002), original data kindly provided by the author. Loess (bulk): Mean of 7 loess samples from various sampling sites in the Loess Plateau south of the Mu Us desert, shown element ratios calculated after original data given in Ding et al. (2001), see also this reference for the sampling locations.

7: Mean of the grain size fractions < 2 and 2–63 μm of 4 loess profiles from uplifted river terraces in the Hexi-Corridor (40 individual samples), calculation of Al_2O_3 on $CaCO_3$-free basis. GPS-sampling locations: (H S1–8, 10–80 cm) 39°45.68′ N, 97°31.40′ E (H S9–15, 10–70 cm) 39°46.11′ N, 97°31.90′ E (H S16–26, 10–110 cm) 39°39.53′ N, 97°40.20′ E (H S27–40, 10–140 cm) 38°47.93′ N, 100°11.03′ E.

a: Analytical measurements performed after high-pressure decomposition, see Section: 'Analytical methods and sample preparation'.

b: Data related to the individual samples given below of the shown La_N/Yb_N values in italic letters, analytical measurements after high-pressure decomposition.

c: There are no significant variations in the shown geochemical signatures that could document relative enhanced in-wash of local debris during wet periods.

Please note (i) normalisation of REE-concentrations related to mean composition of Post-Archean-Australian Shales (PAAS) for data from Taylor and McLennan (1985). Eu/Eu* is calculated deviating from the common rule by $Eu_N/(0.5 \cdot Nd_N + 0.5 \cdot Tb_N)$ to characterise the enrichment of the MREEs Sm, Eu, and Gd relative to PAAS in the shown siliciclastic components and the superimposed distinct enrichment of Eu in the local alkalibasaltic rocks and in the SHL sediments, (ii) Al_2O_3 given in weight% per dry substance, given element ratios are mass ratios, Co/Al and Zn/Al are given in (ppm/wt.%), (iii) numbers in brackets give the standard deviation.

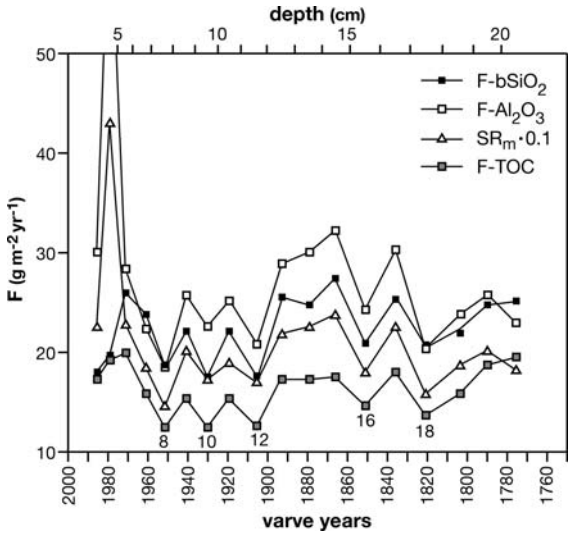

Figure 8. Profiles of geochemical proxies which are positively correlated with the rainfall during the summer monsoon. Calculation of flux rates (SR_m, F-$bSiO_2$, F-Al_2O_3, F-TOC) is based on data given in Table 2. Correlations between individual proxies are shown in Figures 10, 11, and 16a, b. Flux maxima (samples 6, 7, 9, 11, 13–15, 17, 20) represent periods with relatively enhanced climatic wetness. Sample numbers for dry-periods are given below the F-TOC profile.

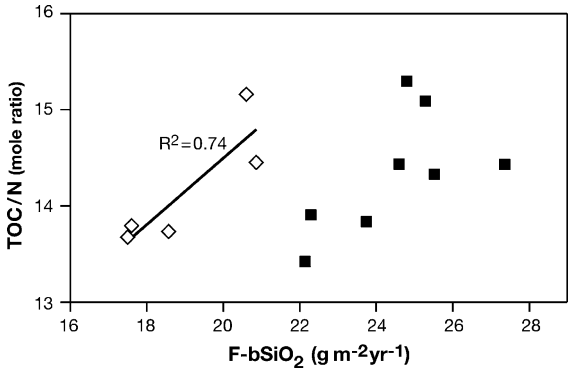

Figure 9. Correlation between F-$bSiO_2$ and TOC/N. Squares: Wet periods, samples 7, 9, 11, 13–15, 17, 20. Diamonds: Dry periods, samples 8, 10, 12, 16, 18; for wet and dry periods see Figure 8.

vegetation. Such a type of vegetation is related to high evapotranspiration during the growing season. Continuous release of algae nutrients in combination with substantial evapotranspiration prevents an exhaustion of the leachable nutrient reservoir of the lake catchment during the rainy season. We therefore can assume also a positive correlation between groundwater inflow from the catchment and influx of algae nutrients. Since rainfall during the summer monsoon mainly feds the local groundwater discharge and the palynological record of Lake SHL documents only minor variations in the assemblage and density of the local woody vegetation during the last centuries (Mingram et al. 2004), conclusively, there should also exist a positive correlationship between the flux of biogenic silica and palaeovariations in summer monsoon rainfall. The tendency towards acidification in the watershed area during the last decades probably affected silicate-weathering in the catchment of the lake. The release and the mobility of phosphorus may have been positively affected by acidification, whereas the dissolved influx of silica could have been lowered by pH decrease in groundwater discharge.

Lake-internal forcing of photosynthetic production

There also exists internal forcing on bio-production by the diffusive reflux of nutrients from the surface sediments and the seasonal nutrient cycle in the dimictic lake. In contrast to phosphate, the diffusive reflux of dissolved silica from the surface sediments is largely unaffected by changes in the redox conditions and can be assumed to be relatively constant. In particular, net accumulation of biogenic opal can not be sustained by postdepositional dissolution of siliceous diatom skeletons and the diffusive Si reflux across the sediment/water interface. However, high enough focussing of the particle flux towards the centre of lake SHL can counterbalance the postdepositional diffusive Si reflux or can even give an internal forced portion of the $bSiO_2$ flux for sediments from the centre of the lake. The nutrient cycling in lake SHL may vary with changes in the hydrological conditions, e.g., subsurface inflow may be associated with temporal upward advective transport of nutrients from the hypolimnion to the phototrophic zone. Such a scenario lowers the lake internal nutrient reflux during the following overturn and will be hardly detectable in individual samples which averages sedimentation over a decade and longer.

In the non-calcareous sediments, inorganic phosphorus is largely immobilised on Fe(Mn)-precipitates. It can be released into the pore water when these precipitates react with H_2S to form sulphides. The production of H_2S by sulphate-reduction is limited by the low concentration of

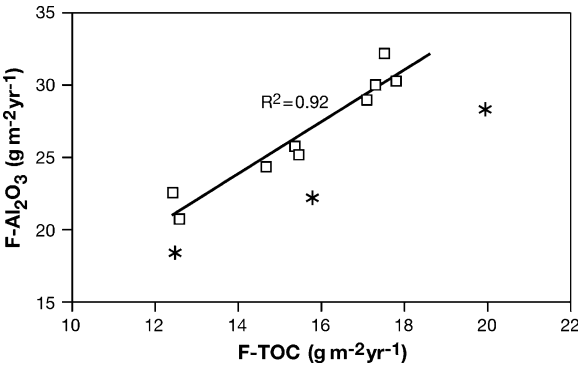

Figure 10. Correlation between mean annual accumulation of TOC (F-TOC) and the flux of Al_2O_3 (F-Al_2O_3) for sediment samples 9–17. In Lake SHL, influx of aluminium silicates and autochthonous deposition are positively correlated. Samples 6, 7, and 8 (asterisks), which document enhanced autochthonous deposition due to eutrophication since ca. 1950, plot below the trend-line defined by older sediment samples.

SO_4^{2-} in the lake (Table 3). The early diagenetic release of phosphorus should depend on the onset and the duration of seasonal anoxic conditions at the sediment/water interface. In general, good varve preservation and no signs for bioturbation in sediments from the centre of the lake basin imply that anoxic conditions prevail in the deep water of Lake SHL. The diffusive reflux of phosphorus might be higher for periods with higher productivity, when enhanced deposition of organic matter increases the O_2-consumption in the hypolimnion. This mechanism may amplify the external forcing of photosynthetic production in the lake. Considering the high inter-annual variability in local summer monsoon rainfall and associated high inter-annual variations in groundwater inflow and all further aspects, discussed above, internal forcing on primary production in Lake SHL can be expected to be much less variable than external forcing on autochthonous biogenic deposition.

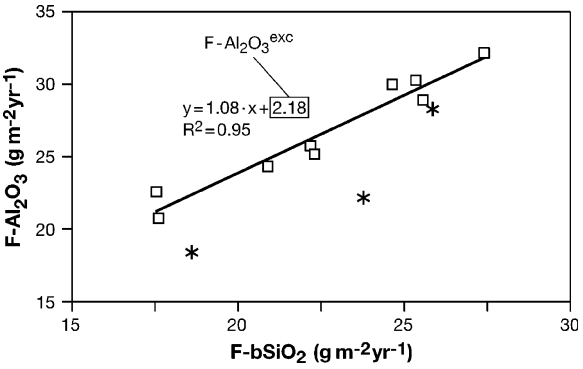

Figure 11. Correlation between F-$bSiO_2$ and F-Al_2O_3 for sediment samples 9–17. Samples 6, 7, 8 (asterisks), which document enhanced autochthonous deposition due to eutrophication since ca. 1950, plot below the trend-line defined by older sediment samples. The F-$bSiO_2$/F-Al_2O_3 ratios for sediments below 8 cm fall close to a value of 1.07. Excess in the influx of Al_2O_3 (F-$Al_2O_3^{exc}$) of 2.18 g m^{-2} yr^{-1} implies that a portion of the siliciclastic input is not positively correlated with rainfall during the summer monsoon.

Balance between various sediment constituents

Balance between 'heavy' allochthonous influx (F-All^{total}) and 'light' autochthonous deposition (F-Au^{total})

The sedimentation record of Lake SHL shows a rather constant ratio between autochthonous deposition and the influx of aluminosilicates, though substantial variations in the mean annual mass accumulation (SR_m), F-TOC, F-$bSiO_2$, and F-Al_2O_3 do exist (Table 2 and Figure 8). In the solid density (ρ_s) – F-Al_2O_3/F-$bSiO_2$ diagram (Figure 12), 'normal' SHL-samples plot in a close cluster with F-Al_2O_3/F-$bSiO_2$ of 1.17 ± 0.04 and ρ_s of 2.29 ± 0.05 g cm^{-3}. The samples 6, 7 and 8 document the modern eutrophication history of the lake with enhanced autochthonous deposition. Sample 7 shows a distinct shift towards lower F-Al_2O_3/F-$bSiO_2$ and lower ρ_s, whereas sample 8, which represents a dry period, has only a lowered F-Al_2O_3/F-$bSiO_2$ value. Sample 6, which documents wetter climatic conditions with relative increased influx of aluminosilicates, plots close to 'normal' SHL-samples. Samples 4 and 5, which document enhanced siliciclastic influx, have F-Al_2O_3/F-$bSiO_2$ values distinctly greater than 1.17 and are characterised by enhanced ρ_s-values. Sample 8 and 10 represent dry periods with a similar decrease of F-TOC and F-$bSiO_2$. Mean annual mass accumulation of sample 10 is less lowered than that of sample 8 (Figure 8). This might document relative enhanced influx of dust by dry-deposition for sample 10. The shift of sample 10 towards higher F-Al_2O_3/F-$bSiO_2$ and ρ_s supports such an interpretation (see Table 2). In the F-$bSiO_2$–ρ_s diagram (Figure 13), sediment samples of dry periods and wet periods define separate clusters for minor variations in ρ_s. The ratio of F-Al_2O_3/F-$bSiO_2$ is rather constant for 'normal' SHL-samples. Sediment genesis on the

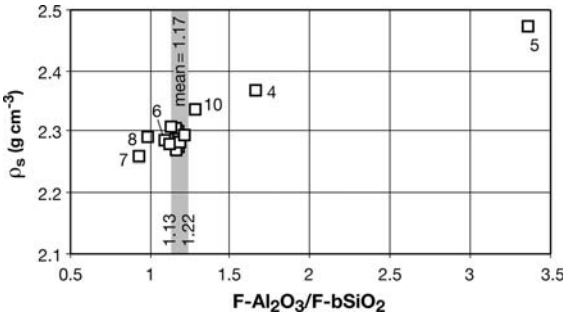

Figure 12. Density of solid sediment (ρ_s) vs. F-Al_2O_3/F-$bSiO_2$ for sediment samples 4–17, numbers of anomalous sediment samples are shown on the diagram. Samples that document enhanced siliciclastic influx by dry-deposition plot to the right of the shaded area, sediment sections which are affected by modern eutrophication show a shift of F-Al_2O_3/F-$bSiO_2$ towards values < 1.17.

conditions of (i) constant F-$bSiO_2$/F-Al_2O_3 ratio of 1.17 (see Figure 12), (ii) All^{total} characterised by 17.5 wt.% Al_2O_3 and $\rho_s(All^{total}) = 2.67$ g cm^{-3}, and (iii) $\rho_s(Au^{total}) = 1.15$ g cm^{-3}, fits the mean solid density of 'normal' SHL-sediments (Figure 14). Variations of ρ_s towards higher values up to 2.47 g cm^{-3} document relatively higher contributions by dry deposited dust for the related sediment sections.

Balance between siliciclastic input of local and remote origin

There are no signs of significant soil erosion in the vicinity of the lake, however, in-wash of local soil particles may occur particularly during heavy rainfall in summer or during the thaw in spring. The interior of the pristine SHL-crater was covered with coarse pyroclastic ejecta of alkalibasaltic composition as the only constituent. These deposits were mixed with siliciclastic particles of remote provenance by continued aeolian deposition. The inorganic fraction of the modern local soils represents a mixture of volcanic rocks, their weathering products, and dust of remote origin with a mineralogical and chemical composition similar to loess. Though the portion of remote debris has become substantial, local soils are still characterised in their bulk chemical and mineralogical composition by the fingerprints of the local alkali-basalts (see Table 4). Geochemical signatures that would make detectable alkalibasaltic rocks and their weathering products in Lake SHL-sediments simply reflect (i) the balance between basic rock constituents and loess (Al/Mg, Al/Ti, Zn/Al, and Co/Al) or (ii) they quantify specific geochemical signatures of the alkali-basalts with a strong contrast against mean loess or mean upper continental crust composition, respectively (Eu_N/Eu_N^*, La_N/Yb_N, K/Na, Rb/Cs). If in-wash of local soil particles by surface run-off during the summer monsoon is significant should become obvious by the comparison of the above geochemical signatures in sediments from dry and wet periods. There is no evidence for relatively increased influx of local siliciclastic matter during wet periods by the parameters Mg/Al, Eu/Eu^*, Al/Ti, Rb/Cs, K/Na, and Zn/Al which closely correspond for wet and dry sedimentation intervals. Only the increase of Co/Al for wet sedimentation intervals might support enhanced influx of alkalibasaltic debris for a stronger summer monsoon (Table 4).

In the following, we use geochemical mass balance to estimate the contribution of local soil erosion by surface run-off to the bulk siliciclastic influx. The REE-characteristics of a selected SHL-sediment sample, and of various materials of local and remote provenance that may contribute to the siliciclastic influx of the lake are shown in Figures 15a and b. Figure 15c shows exemplarily two different mass balances, which give correspondence with the La/Yb and Eu/Eu^* ratios of the SHL-sediment sample. The clay-sized debris from the soil profile S2 (Figure 1b) is considered in both cases as the local component. Model-mix (1) considers 30% local debris and 70% loess from the central loess plateau ($< 20\,\mu m$ fraction). Model-mix (2) considers the $< 2\,\mu m$ fraction of non-calcareous loess from an uplifted river terrace in Changchun (47%). The clay-size fraction of this loess, however, is characterised by a distinct negative Ce-anomaly, which is not obtained in the SHL sediments. The silt fraction is modelled by

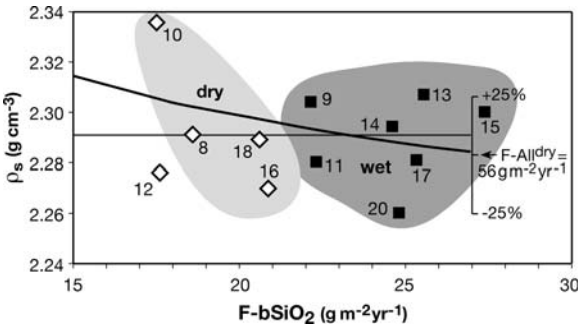

Figure 13. Flux of biogenic silica (F-bSiO$_2$) vs. ρ_s (samples 8–20). Individual sediment samples representing wet and dry periods, respectively, define separate sample clusters for rather constant values of ρ_s. This documents coinciding variability in the accumulation of 'light' autochthonous deposits and in the influx of heavy siliciclastic debris. *Horizontal line*: Mean ρ_s of samples 8–20. *Solid curve*: Hypothetical correlation between F-bSiO$_2$ and ρ_s for constant influx of siliclastic debris by dry deposition (F-All^{dry} = 56 g m^{-2} yr^{-1}) for the following assumptions: F-Au^{total} = F-bSiO$_2$·2.2, F-All^{wet} = (F-bSiO$_2$ – 5.5)·1.082·(100/19.6), ρ(Au^{total}) = 1.15 g cm^{-3}, ρ(All^{wet}) = ρ(All^{dry}) = 2.67 g cm^{-3}. Please note that the factor 1.08 is given by the gradient of the trend line in the F-bSiO$_2$–F-Al$_2$O$_3$ diagram (Figure 11). The insert scale gives resulting ρ_s-values at 20% higher and lower dust influx by dry-deposition for F-bSiO$_2$ = 27 g m^{-2} yr^{-1}.

the 2–63 µm fraction of a sand dune from Horqin Shadi (28%). Local siliciclastic influx accounts for 25% in this estimate.

Aeolian influx by dry- and wet-deposition

The major portion of the siliciclastic sediment fraction originates from the aeolian influx of dust.

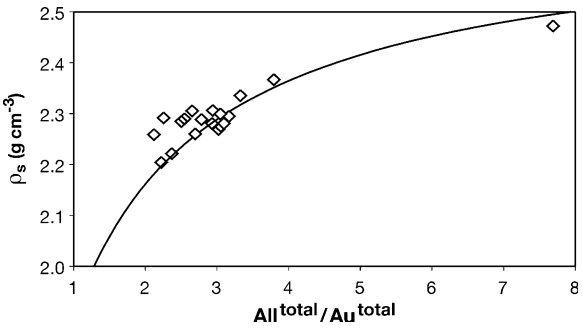

Figure 14. Model for the density of the solid sediment (ρ_s) in Lake SHL. Dependence of ρ_s on the ratio between the bulk allochthonous siliciclastic (All^{total}) and the bulk autochthonous sediment fraction (Au^{total}), ρ(Au^{total}) = 1.15 g cm^{-3}, ρ(All^{total}) = 2.67 g cm^{-3}. *Open diamonds*: Individual samples between 4 and 22 cm, considered parameters for presentation: Au^{total} = bSiO$_2$·x (x = 2.2 below 9 cm, x = 2.5 above), All^{total} = Al$_2$O$_3$·17.5 (4–17 cm), All^{total} = 100 – Au^{total} (below).

Local debris and chemical precipitation of the inorganic dissolved influx contribute only in a minor portion to annual mass accumulation (SR$_m$). Out-wash of atmospheric mineral aerosols and in-wash of local soil particles increase with increase in precipitation. If substantial portions of the autochthonous and allochthonous sediment fraction are not positively correlated with the rainfall during the summer monsoon, this should become detectable in the highly correlative trends between F-bSiO$_2$ and F-Al$_2$O$_3$ (samples 9–17, R^2 = 0.95, Figure 11) or between F-bSiO$_2$ and SR$_m$ (samples 9–20, R^2 = 0.85, Figure 16a), respectively.

Dust-influx by wet-deposition and in-wash of soil particles during the rainy season should be positively correlated with the summer monsoon strength, whereas aeolian influx by dry-deposition is independent of local precipitation. Neither does there exist a direct correlationship between in-wash of local soil particles by surface run-off during the thaw in spring and summer monsoon. For simplification, we will consequently call the portion of the total siliciclastic flux, which is assumed to be positively correlated with the summer monsoon strength, F-All^{wet} (wet deposited dust flux) and the siliciclastic influx, which is independent from rainfall during the summer monsoon F-All^{dry} (dry deposited dust flux).

The net accumulation of biogenic silica at the centre of the lake basin (F-bSiO$_2$) shows interannual variability mainly by variable inflow of nutrient-rich groundwater. The biogenic uptake of the diffusive Si reflux from the surface sediments of the whole lake basin by diatoms results in an additional contribution to the net accumulation of biogenic silica at the flat lake bottom due to focussing of the particle flux towards the centre of the U-shaped lake basin. Lake-internal processes less influence the diffusive reflux of Si from the surface sediments, we therefore can assume that the contribution to F-bSiO$_2$ by internal forcing is relatively constant. We use the above correlations to estimate the balance between F-All^{wet} and F-All^{dry} for hypothetical (constant) contributions through internal forcing on autochthonous biogenic deposition.

F-bSiO$_2$–F-Al$_2$O$_3$. The highly correlative trend between F-bSiO$_2$ and F-Al$_2$O$_3$ for samples 9–17, shown in Figure 11, documents an excess in F-Al$_2$O$_3$ of 2.18 g m^{-2} yr^{-1} which implies that mass-accumulation by dry deposition of dust exceeds

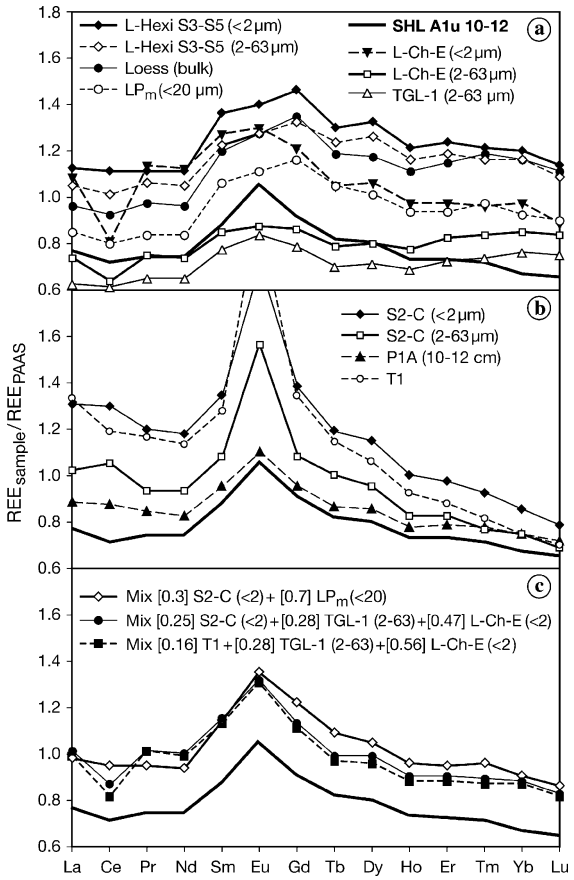

Figure 15. PAAS-normalised REE-concentrations of SHL-sediments (Alu 10–12), of selected aeolian deposits from China, and of local components from the Long Gang area (see Figure 1 for locations), REE-concentrations of PAAS after Taylor and McLennan (1985), shown analytical data measured in our laboratory are all based on measurements after decomposition under high pressure conditions (see Section 4), see Table 4 for additional sample information. (a) *Loess (bulk)*: Mean of bulk Loess from the Central Loess Plateau calculated on volatile-free basis, data from Ding et al. (2001), LP_m(< 20 µm): Mean of 11 loess samples (< 20 µm fractions, volatile-free) from the Central Loess Plateau, same samples as published in Sun (2002), original analytical data kindly provided by the author, *L-Hexi (S3-S5)* (< 2 µm) and (2–63 µm): Grain size fractions of calcareous loess samples from the Hexi-Corridor near Yumen (39°45.68′ N, 97°31.40′ E, calculated on $CaCO_3$-free basis, *L-Ch-E* (< 2 µm) and (2–63 µm): Grain size fractions of a non-calcareous loess sample from Changchun, *TGL-1* (2–63 µm): Silt fraction of a sand dune sample from Horqin Shadi. (b) *S2-C* (< 2 µm) and (2–63 µm): Selected grain size fractions of a local soil sample, *P1A (10–12 cm)*: Bulk composition of a nearby soil profile between 10 and 12 cm depth, *T1*: local tephra, see Table 4 for further explanations. (c) Synthetic PAAS-normalised REE-concentrations obtained by two or three component mix of selected local and remote siliciclastic components that fit the obtained Eu/Eu*-anomaly of SHL-sediments, considered weight-proportions are given in brackets before the components.

the internal forced portion of the biogenic silica flux (F-$bSiO_2^{int}$). The siliciclastic influx, which does not depend on rainfall during the summer monsoon (F-All^{dry}) would account for 12.5 g m^{-2} yr^{-1} if F-$bSiO_2^{int} = 0$, and a Al_2O_3 concentration of 17.5 wt.% for the siliciclastic sediment constituent were considered.

F-$bSiO_2^{corr}$–F-Al_2O_3. In the following, the external forced flux of biogenic silica is calculated for hypothetical values of F-$bSiO_2^{int}$ by F-$bSiO_2^{corr}$ = F-$bSiO_2^{total}$ – F-$bSiO_2^{int}$. The derived F-$Al_2O_3^{exc}$ values, which estimate the influx of Al by dry-deposition of dust, are positive linear correlated

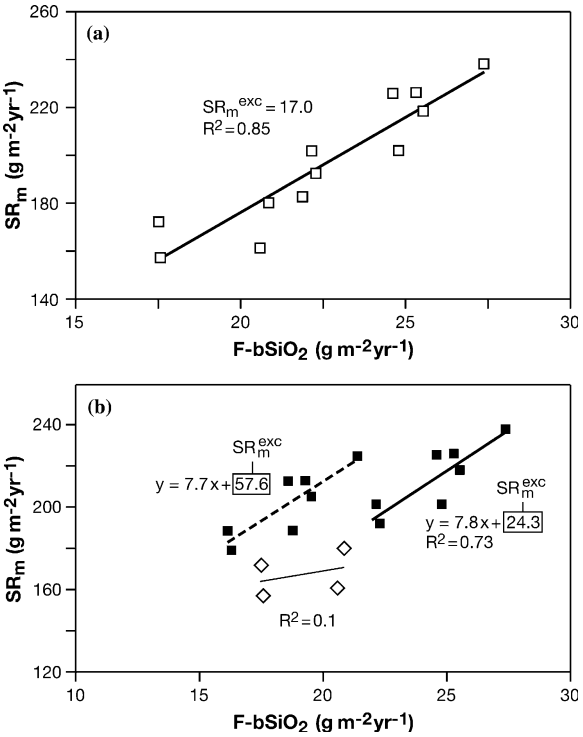

Figure 16. (*Upper diagram*) Correlation between F-$bSiO_2$ and mean annual mass accumulation (SR_m) for samples 9–20, the shown trend-line documents excess in SR_m (SR_m^{exc}) of 17.0 g m^{-2} yr^{-1} which is not positively correlated with rainfall. (*Lower diagram*) Same correlation for wet (squares) and dry periods (diamonds) separately. The SR_m^{exc} for individual sediment samples from wet periods is 24.3 g m^{-2} yr^{-1}. The dashed trend-line shows the correlation for the sample clusters if hypothetical contributions on bulk autochthonous deposition by internal forcing are corrected by subtraction. The value for F-$bSiO_2^{int}$ taken into account is 6 g m^{-2} yr^{-1}, F-Au^{int} is estimated by 2.2·F-$bSiO_2^{int}$. The excess in SR_m increases by such a correction which implies that SR_m^{exc} must be substantially related to aeolian influx of dust by dry-deposition.

with F-$bSiO_2^{int}$. Aeolian siliciclastic input by dry-deposition may deviate in its chemical composition from the influx of dust scavenged by wet-deposition. Figure 17 demonstrates the relation between F-All^{dry} and F-$bSiO_2^{int}$ for hypothetical Al_2O_3 concentrations of the dry deposited dust fraction (thin dashed lines).

F-$bSiO_2^{corr}$–SR_m. F-All^{dry} can be also estimated by the SR_m^{exc} in the F-$bSiO_2^{corr}$–SR_m correlation for corrected values of SR_m. We consider F-$bSiO_2^{corr}$ = F-$bSiO_2^{total}$ − F-$bSiO_2^{int}$ for the external forced flux of biogenic silica as above, and correct Sr_m for the internal forced autochthonous deposition rate (F-Au^{int} = 2.2·F-$bSiO_2^{int}$) $SR_m^{corr1} = SR_m$ − F-Au^{int}. The solid line shown in Figure 17 gives the correlation between F-All^{dry} and hypothetical values of F-$bSiO_2^{int}$. Probable couples of F-$bSiO_2^{int}$ and $Al_2O_3[All^{dry}]$ (Al_2O_3 concentration of the dry deposited dust fraction) are given by the intersections of this line with the individual lines derived from correlation between F-$bSiO_2^{corr}$ and F-Al_2O_3 (see above). There is a limited variation range for $Al_2O_3[All^{dry}]$ which gives correspondence between the two estimates (8–16.5 wt.% Al_2O_3).

Combined iterative approach. In an alternative iterative approach, we estimate F-Au^{int} and F-$bSiO_2^{corr}$ for hypothetical values of F-$bSiO_2^{int}$ in the same way as above. A first iterative step considers the correlation between F-$bSiO_2^{corr}$ and corrected values for SR_m: $SR_m^{corr2} = SR_m$ − F-Au^{int} − F-All^{dry}. SR_m^{corr2} represents the hypothetical values for mean annual mass accumulation that could be obtained if no influx of dust by dry-deposition and internal forcing on autochthonous deposition were present. For hypothetical values of F-$bSiO_2^{int}$, we determine the values of F-All^{dry}, which force the trend lines in the individual F-$bSiO_2^{corr}$ – SR_m^{corr2} correlations through zero, by iteration. The balanced F-All^{dry} values are used to calculate the Al_2O_3 influx by wet deposition of dust: F-$Al_2O_3^{wet}$ = F-$Al_2O_3^{total}$ − ($Al_2O_3[All^{dry}]$·100/F-All^{dry}). In a second iterative step, we determine the Al_2O_3 contents of the dry deposited dust fractions $Al_2O_3[All^{dry}]$ which force the trend lines in the correlations between F-$Al_2O_3^{wet}$ and SR_m^{corr2} through zero. The balanced data allow to calculate the Al_2O_3 contents of the wet deposited dust fractions $Al_2O_3[All^{wet}]$ and the values of F-All^{wet}/F-All^{dry} for the individual sediment samples (Table 5). The balanced F-All^{wet}/F-All^{dry} values of samples that represent dry periods are lower than those for samples of wet periods. The balanced F-All^{dry} values show a positive linear correlation with the assumed values of F-$bSiO_2^{int}$ (Figure 17). They may vary between ca. 25 and 90 g m^{-2} yr^{-1} which corresponds with a variation range of F-All^{wet}/F-All^{dry} between 4.9 (F-$bSiO_2^{int}$ = 0 g m^{-2} yr^{-1}) and 0.6 (F-$bSiO_2^{int}$ = 12 g m^{-2} yr^{-1}) (Table 5). The derived values for F-$Al_2O_3^{wet}$ and F-$bSiO_2^{corr}$ (external forced flux of biogenic silica) show similar variability (max. ± 50%). The Al_2O_3 concentrations of the balanced dry deposited dust fractions ($Al_2O_3[All^{dry}]$) vary between 8.2 wt.% (F-$bSiO_2^{int}$ = 0) and 16.4 wt.% (F-$bSiO_2^{int}$ = 12 g m^{-2} yr^{-1}) (Figure 18). Aeolian siliciclastic influx originating from wet-deposition is characterised by higher Al_2O_3 contents. The mean Al_2O_3 concentration of the wet deposited dust fraction ($Al_2O_3[All^{wet}]$) is 19.6 wt.% (Table 5), concentrations in this order of magnitude are characteristic for siliciclastic matter with high contents in clay minerals.

As a part of this study a number of loess and sand dune deposits from remote regions west of Lake SHL were analysed for their chemical composition (Table 4). The clay-fractions of non-calcareous loess-like deposits near Changchun (Figure 1), for instance, are characterised by Al_2O_3 concentrations of 18.8–19.8 wt.%. The silt-fractions (2–63 μm) of

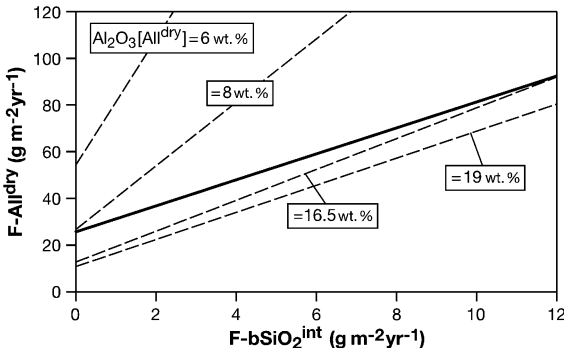

Figure 17. Various estimates for the influx of dust by dry-deposition (F-All^{dry}). *Thick line*: Based on SR_m^{exc} in the correlation between F-$bSiO_2$ and SR_m (samples 9–17) for assumed different portions of internally forced autochthonous deposition (F-Au^{int}, F-Au^{int} = 2.2·F-$bSiO_2^{int}$). *Thin dashed lines*: Based on the excess of F-Al_2O_3 in the correlation between F-$bSiO_2$ and F-Al_2O_3 for assumed same values of F-$bSiO_2^{int}$ and hypothetical Al_2O_3-concentrations for the dry deposited dust fraction ($Al_2O_3[All^{dry}]$). The probable range of $Al_2O_3[All^{dry}]$ (8–16.5 wt.%) is defined by the intersections of the thin dashed lines with the thick line.

investigated sand dune samples from the Horqin Shadi (Figure 1) and the silt fractions of the loess samples from Changchun have Al_2O_3 contents between 11.0 and 11.9 wt.% (Table 4). $Al_2O_3[All^{dry}]$ values in this order of magnitude correspond with a F-$bSiO_2^{int}$ value of 2 g m^{-2} yr^{-1} in the above mass balance estimates (Figure 18).

The Si balance of Lake SHL

In the sedimentation record from the centre of the Lake SHL, mean annual mass accumulation (SR_m), total siliciclastic influx (F-All^{total}), and the net accumulation of biogenic silica (F-$bSiO_2$) and TOC (F-TOC) are positively correlated with rainfall during the summer monsoon. Each of these fluxes include components that do not correlate with the rainfall during the summer monsoon, for instance, the aeolian influx of dust by dry-deposition (F-All^{dry}) or the portion of F-$bSiO_2$, that is related to the lake-internal forcing of diatom production (F-$bSiO_2^{int}$).

Geochemical mass balances based on the correlation of the above proxies were used to estimate the siliciclastic influx which does not depend on rainfall during the summer monsoon (F-All^{dry}) (see above). The balanced values for F-All^{dry} depend on hypothetical values of F-$bSiO_2^{int}$. For mass balance estimates based on sediment data alone, a wide range of F-$bSiO_2^{int}$ (0–12 g m^{-2} yr^{-1}) is probable, which corresponds with a Al_2O_3 concentration range between 8 and 16.5 wt.% for the dry deposited dust fraction (All^{dry}) and with a F-All^{wet}/F-All^{dry} ratio between 0.6 and 4.9 (Table 5). In the following, hydrochemical monitoring data of the lake and the groundwater discharge are used to get an improved understanding of the balance between external and internal forcing on the net accumulation of biogenic silica at the centre of the lake basin.

General model assumptions

The nearly circular lake is divided into three depth sections (Figure 19): section I (0–15 m), section II (15–50 m), section III (50 m, flat bottom). We assume that the diffusive reflux of dissolved silica from the surface sediments F-$SiO_{2(refl)}$ is constant and equal for all depth sections. We further assume that all depth sections receive uniform dissolved influx of silica by inflow of groundwater. Since uptake of dissolved silica by diatoms is restricted to the upper section, dissolved Si is accumulated during the stratification periods below 15 m water depth (Si^{accum}). The proportion of Si^{accum} that becomes bio-available by seasonal overturn can be roughly estimated by: Si^{accum}. $[V_{Lake}{}^{0-15m}/(V_{Lake}{}^{total} + V^{inflow})]$. Sediment accumulation in sections I and II is assumed to be lower than for the flat lake bottom. The portion of the diffusive Si reflux from the depth sections I and II, which is seasonally transferred in biogenic silica

Table 5. Estimation and characterisation of dust input by dry- and wet-deposition for hypothetical values of F-$bSiO_2^{int}$.

F-$bSiO_2^{int}$ [a]	0		2		4		6		8		12	
F-All^{dry} [a]	25.7		36.9		48.0		59.1		70.3		92.5	
$Al_2O_3[All]^{dry}$	8.16		11.59		13.43		14.57		15.35		16.35	
Sampl.	x [b]	y	x [b]	y	x [b]	y	x [b]	y	x [b]	y	x [b]	y
9	18.6	4.9	18.5	3.1	18.4	2.2	18.3	1.6	18.1	1.2	17.6	0.7
10*	19.0	4.2	18.9	2.6	18.3	1.8	18.8	1.3	18.6	0.9	18.1	0.4
11	19.6	4.6	19.7	2.9	19.7	2.0	19.7	1.4	19.7	1.0	19.8	0.5
12*	20.1	3.6	20.2	2.2	20.3	1.5	20.5	1.0	20.7	0.7	21.7	0.3
13	19.7	5.3	19.7	3.4	19.7	2.4	19.7	1.7	19.7	1.3	19.8	0.8
14	19.1	5.7	19.1	3.7	19.0	2.6	19.0	1.9	18.9	1.4	18.7	0.9
15	19.8	5.9	19.8	3.8	19.8	2.7	19.8	2.0	19.9	1.5	19.9	0.9
16*	20.5	4.2	20.6	2.6	20.8	1.8	20.9	1.3	21.2	0.9	22.1	0.4
17	19.5	5.6	19.5	3.6	19.5	2.5	19.5	1.9	19.5	1.4	19.4	0.8
m. (9–17)	19.5	4.9	19.5	3.1	19.6	2.2	19.6	1.6	19.6	1.2	19.7	0.6

[a]: Flux rates (F-) in (g m^{-2} yr^{-1}), $bSiO_2$: biogenic silica, All^{dry}: siliciclastic sediment fraction originating from dry-deposition of dust.
[b]: Concentrations given in weight% per dry substance.
x: $Al_2O_3[All^{wet}]$: Balanced Al_2O_3 concentrations of the wet deposited dust fractions (combined iterative approach).
y: F-All^{wet}/F-All^{dry}: Balance between wet and dry depositional influx of dust.
*: Marked samples represent dry periods (see Figure 8); and are characterised by lower F-All^{wet}/F-All^{dry} values.

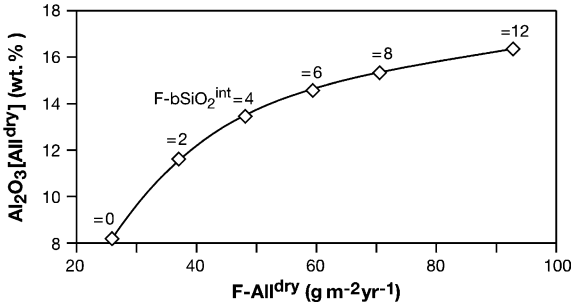

Figure 18. Geochemical mass balances to quantify the influx of dust by dry-deposition and to characterise its chemical composition. Combined iterative approach based on geochemical data of SHL sediment samples 9–17 (see Section 'Aeolian influx by dry- and wet-deposition' for explanations). Correlation between balanced values for F-All^{dry} and the Al_2O_3 concentration of the dry deposited dust fraction (Al_2O_3[All^{dry}]) for hypothetical values of F-bSiO_2^{int}.

and settles by focussing of the particle flux at the flat lake bottom is called F-bSiO_2^{int}. Enhanced sediment accumulation at the centre of the lake basin is considered by the focussing factor [F_{focus} = (Sediment accumulation rate in depth section III)/(Hypothetical sediment accumulation rate if each depth section receives the same particle flux)]. Focussing of sediment accumulation towards the centre of the lake basin could reach theoretically a maximum value of 8.5, if no sediment accumulation in depth-sections I and II was present. The total area of the lake basin in the depth sections I (shallow depth sections with convection) and II (steeply inclining part of the lake basin), which may be affected by reduced sediment accumulation, exceeds the area of depth section III (flat lake bottom) by a factor of 7.45 (Figure 19). A minor focussing of settling particles towards the centre of the lake is therefore related to a substantial increase of F_{focus} above 1. In the case of F_{focus} = 2.5, for instance, the sediment accumulation rate for the depth sections I and II is only by 20% reduced.

Lake internal cycling of Si

Estimates of the diffusive reflux of dissolved silica are based on the 1st Fick's law. The considered Si-concentration gradient of 2.5 (μg cm^{-3}) cm^{-1} was obtained by *in-situ* pore water measurements in the surface sediments of a similar Maar lake (Germany: Meerfelder Maar; Schettler, unpublished data). The total diffusive flux of dissolved SiO_2 from the surface sediments is $1.61 \cdot 10^6$ g per annum, which corresponds to a flux rate of 3.9 g m^{-2} yr^{-1}. The portion of the diffusive SiO_2-reflux that becomes bio-available can be estimated by F-$SiO_{2(refl)} \cdot (A_{Basin}^{0-15\ m} + A_{Basin}^{<15\ m} \cdot V_{Lake}^{0-15\ m}/V_{Lake}^{total})$. It would account for $1.16 \cdot 10^6$ g SiO_2 per year or 72% of the total Si reflux, if no loss of Si by the outflow occurred. Without focussing of sediment accumulation towards the centre of the lake basin, no net flux of biogenic silica by internal forcing is present at the flat lake bottom (F-bSiO_2^{int} = 0). If the Si reflux that becomes bioavailable is quantitatively transferred in diatomaceous matter, a net-accumulation of biogenic silica by internal forcing is present for F_{focus} values larger than 1.38; F_{focus} = 2.1, for instance, corresponds to a F-bSiO_2^{int} value of 2 g m^{-2} yr^{-1}. According to geochemical mass-balances based on geochemical sediment composition, the maximum value of F-bSiO_2^{int} might be hypothetically 12 g m^{-2} yr^{-1}. This value is realised for F_{focus} = 5.7. Sediment accumulation at the flat lake bottom exceeds that in depth sections I and II by a factor of 15.4 for this hypothetical case.

External input of dissolved Si

Dissolved Si concentrations in groundwater discharge from September 1999 and June 2001 show only minor variations (13.4 and 12.0 mg l^{-1} Si). Influx of dissolved silica by groundwater discharge, largely related to seepage of rain during MJJASO (EVPT = 85%), and minor contributions by precipitation onto the lake surface accounts together for ca. 47% of the dissolved SiO_2-inventory of the modern lake which becomes bioavailable by seasonal overturn (Figure 19). The external forcing of production and deposition of biogenic silica by groundwater formation in the course of the summer monsoon, therefore must be substantial. Total precipitation during the summer monsoon P[MJJASO] shows distinct inter-annual variability (Table 1) with a relative standard deviation of 22% for the monitoring period 1955–1997. Local groundwater discharge is controlled by rainfall during the summer monsoon (see Section 'External forcing of photosynthetic production'). We assume, that precipitation during winter monsoon (NDJFMA, 114 mm), when the top soils are frozen, contributes only in a negligible proportion to the groundwater discharge. About half

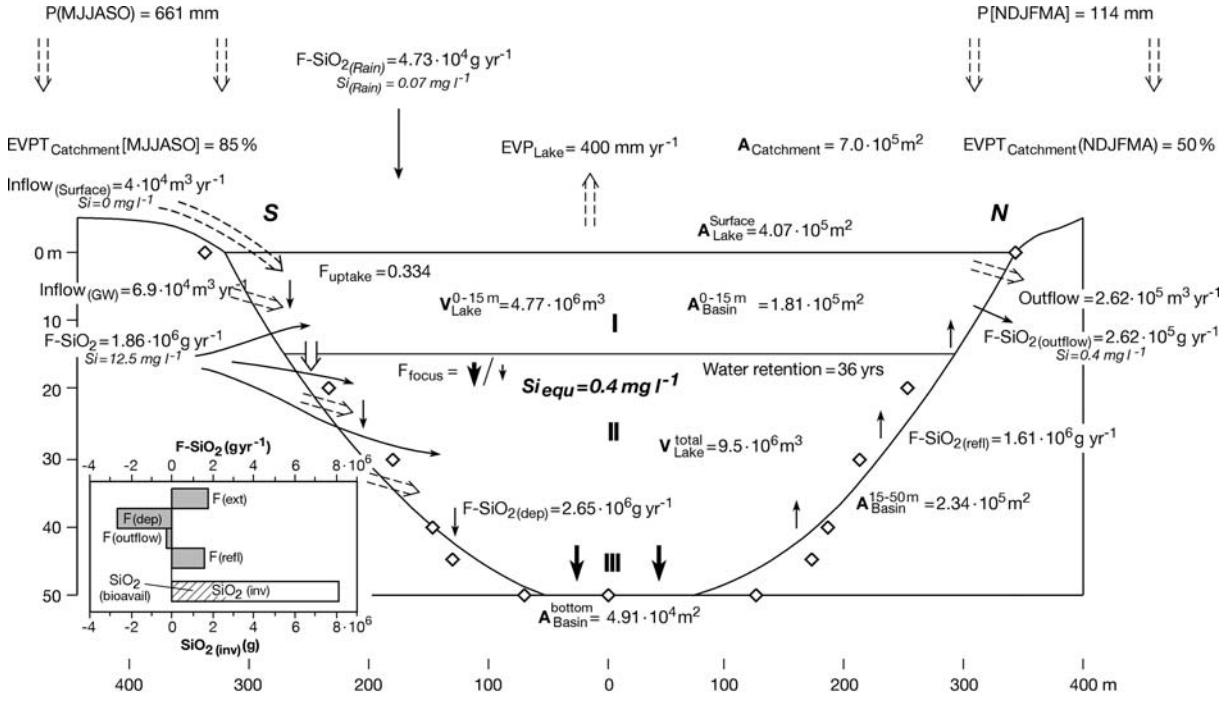

Figure 19. South–North profile of Lake SHL. Schematic setting demonstrates the water budget and annual flux rates of SiO_2 between the various compartments of the aquatic system for assumed stationary conditions. Data on volumes and areas for the lake basin are based on field measurements carried out during the field campaigns (diamonds), data on flux rates largely correspond with hydrological Case 2 (Figure 20b, see also Section 'The Si balance of Lake SHL'). We assume that 50% of the external SiO_2-influx are completely transferred into diatomaceous matter. The bulk biogenic uptake rate (F_{uptake}) of the other 50% portion which fits the obtained Si equilibrium-concentration of the mixed lake is 0.334. The inserted diagram demonstrates the SiO_2-balance for Case 2 and $EVPT[MJJASO]_{Catchment}$ = 85%. Note: (1) The proportion of SiO_2 which gets lost by sub-surface outflow is only minor. (2) The bulk influx of SiO_2 by groundwater inflow and direct precipitation onto the lake surface [$F\text{-}SiO_{2(ext)}$], and the bulk diffusive reflux of SiO_2 across the sediment/water interface ($F\text{-}SiO_{2(refl)}$) are of a similar order of magnitude. (3) Since inflow of groundwater proceeds preferentially into the productive upper depth section, the bio-availability of $F\text{-}SiO_2$(ext) is higher than for the dissolved SiO_2 inventory.

of the total precipitation between November and April may evaporate (see for instance, data on the direct evaporation from the snow cover of Lake Mendota, Wisconsin, 0.029 mm h^{-1} for 10 h per day, Warnecke 1991), and a further substantial proportion may discharge by surface run-off into the lake during the thaw in April. We assume that the surface run-off makes negligible contributions to dissolved silica influx. Dissolved silica concentration in precipitation of a single rainfall event during the summer monsoon was 0.07 mg l^{-1} Si. We further assume that the obtained Si concentration is in equilibrium with wet-scavenged mineral particles and no further release of silica proceeds during the settling of these particles.

Biogenic uptake of Si

In our model, the biogenic uptake rate of dissolved Si in depth section I (F_{uptake} = 0…1) can be estimated on the basis of the Si concentrations measured in the modern lake. We assume that the Si concentration of the modern (mixed) lake is close to steady-state, and approximate the Si concentration of the mixed lake (Si_{equ}) by the mean Si concentration of the water column obtained at the end of the summer stratification (0.4 mg l^{-1}, see Figure 4). In the following, F_{uptake} values are calculated for 4 different scenarios.

Case 1: External Si influx only. Figure 20a shows the adjustment of Si_{equ} in an initially Si-depleted lake for various EVPT-values when only external input of dissolved Si by the groundwater discharge (12.5 mg l^{-1}) and by direct precipitation onto the lake-surface (0.07 mg l^{-1}) are taken into account. The Si_{equ} value of the modern lake and EVPT = 85% could be obtained for a rather low uptake factor (F_{uptake} = 0.168), if 50% of winter precipitation in the catchment were considered as

surface run-off with negligible concentrations in dissolved silica.

Case 2: External Si influx and diffusive Si reflux from the surface sediments. Considering additional contributions by the diffusive flux of Si from the surface sediments (3.9 g m^{-2} yr^{-1}) accounts for a F_{uptake} value of 0.382 at EVPT = 85% to obtain Si_{equ} of the modern mixed-lake (Figure 20b).

Case 3: Additional Si influx by winter precipitation. Cases 1 and 2 do not consider any influx of dissolved Si from the catchment related to precipitation during the winter monsoon (NDJFMA). We assumed in these cases that 50% of winter precipitation discharges by surface run-off with negligible concentrations of dissolved Si into the lake. Considering this amount as sub-surface inflow with an dissolved Si concentration of 12.5 mg l^{-1} increases the balanced F_{uptake} value to 0.427 (Figure 20c).

Case 4: Internal Si reflux only. Figure 20d shows the adjustment of Si_{equ} in an initially Si-depleted lake when the diffusive reflux of Si from the surface sediments is considered as only source for the input of dissolved Si. The considered Si source is constant and therefore not correlated with the inflow of groundwater. The balanced values of F_{uptake}, which fit the Si concentration of the mixed lake vary only slightly for changes in the groundwater discharge; F_{uptake} is 0.28 for EVPT = 85%.

Probably, case 2 (Figure 20b) for EVPT = 85% most closely fits the real conditions in Lake SHL. The balanced biogenic uptake of dissolved Si in Lake SHL for this case accounts for 53% of the hypothetical portion (72%) of lake-water dissolved Si, which becomes bioavailable by seasonal overturn. Without consideration of sediment focussing, the parameter setting of case 2 gives a depositional flux of biogenic silica of 3.2 g m^2 yr^{-1} for the whole lake bottom. The balanced net accumulation rates of biogenic silica (F-$bSiO_2$) for the sediments of the flat lake bottom are much higher than this value and demand for a substantial focussing of the particle flux towards the flat lake bottom. Before we will finally estimate sediment focussing in Lake SHL, we will critically inspect the major assumptions of our Si balance model, in the following, and will asses the sensitivity of the Si mass budget to variations in the parameter setting.

Verification of model assumptions

The sedimentation period (1830–1947, samples 9–17) was influenced neither by enhanced siliciclastic influx, as obtained around 1980, nor by modern eutrophication. Therefore, we focus the mass balance estimates on this sedimentation interval. Mean annual accumulation of biogenic silica (F-$bSiO_2^{total}$) for the balanced sediment section (samples 9–17) varied between 17.5 and 27.4 g m^{-2} yr^{-1} (Figure 8 and Table 2). These values may slightly overestimate the real accumulation rate of diatomaceous silica for analytical reasons, since minor amounts of silica are released from the siliciclastic sediment fraction during the leaching with hot 2 M Na_2CO_3-solution (see Section: 'Analytical methods and sample preparation'). Case 2 (Figure 20b), external influx of Si mainly by inflow of groundwater, and diffusive reflux of Si from the surface sediments, EVPT = 85%, F_{uptake} = 0.382, (F-$SiO_{2(refl)}$ = 3.9 g m^{-2} yr^{-1}) demands a rather high focussing of the particle flux towards the flat lake bottom ($F_{focus} > 6.47$) to obtain a net flux of biogenic silica > 17 g m^{-2} yr^{-1} at the flat lake bottom. Sediment accumulation in depth sections I and II of the lake basin is reduced by 73% for this assumption. If additional dissolved influx of Si from winter precipitation was present (Case 3, EVPT = 85%, Figure 20c), F-$bSiO_2^{total}$ > 17 g m^{-2} yr^{-1} could be balanced for $F_{focus} > 4.65$.

Biogenic uptake of Si. Mass balances for the depositional flux of biogenic silica based on hydrochemical data strongly depend on the assumed value of F_{uptake}. In our model, biogenic uptake of dissolved silica is limited to the upper 15 m of the water column, which accounts for ca. 50% of the total lake-water volume. Hydrochemical profiles obtained during various stages of the summer stratification document nearly complete exhaustion of Si at various depth levels of the epilimnion. A relatively enhanced primary production (Si-minima) at 10 m water depth was reached, for instance, in mid of September 1999 which likely reflects temporary increase of diatom growth due to increased P-availability (originating from inflow of groundwater) at this depth level (Figure 4). We assume that the Si concentration of the mixed water body (0.4 mg l^{-1}) is approximated by the mean Si concentration of the water column at the end of the summer stratification (Figure 4). Estimates of the biogenic uptake of dissolved silica

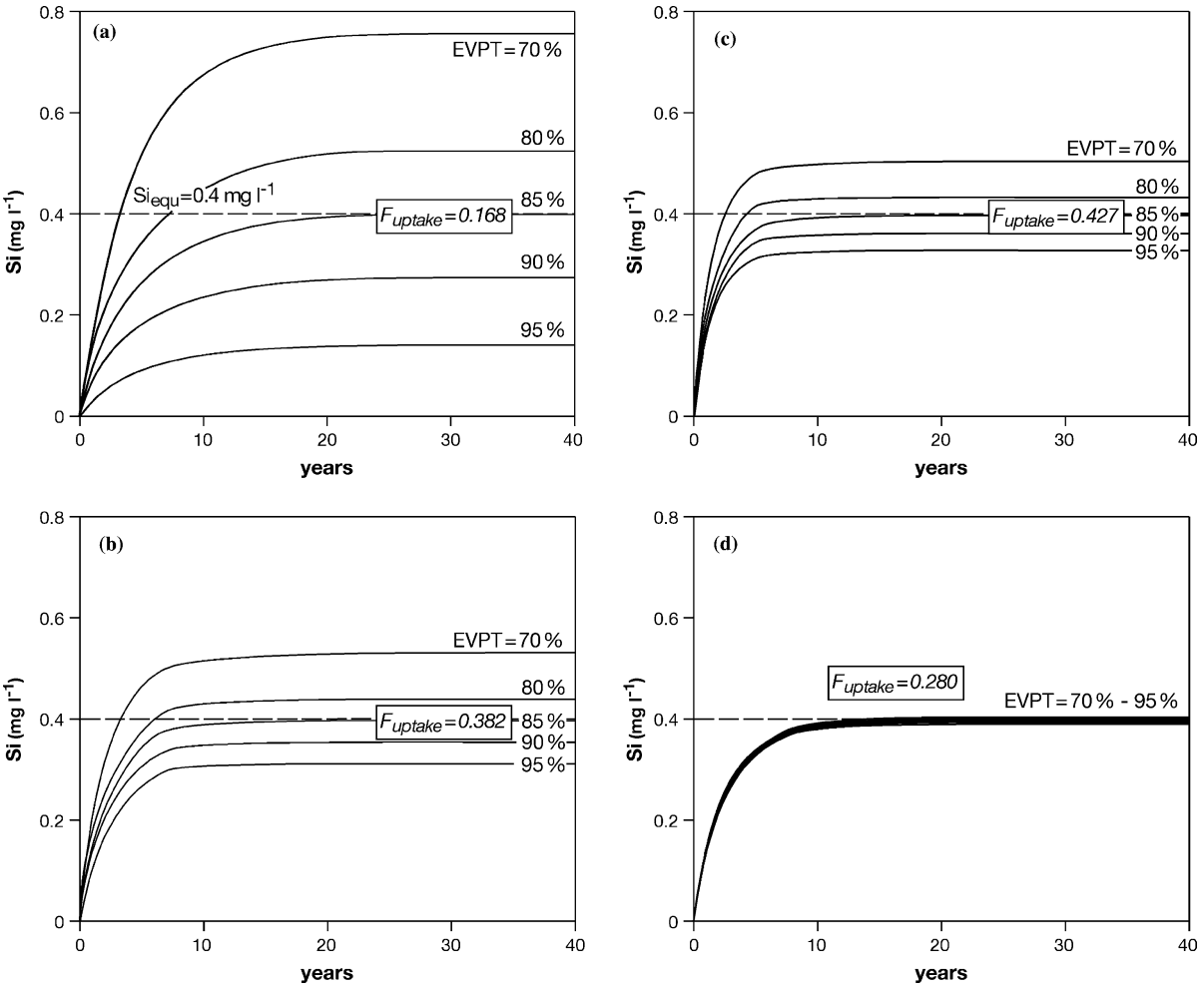

Figure 20. Adjustment of Si equilibrium concentrations (Si_{equ}) in Lake SHL for various values of EVPT during MJJASO. (a) Same hydrological conditions as in Figure 5a, diffusive reflux of Si from the surface sediments not considered. The considered biogenic uptake rate for dissolved Si (F_{uptake} = 0.168) fits a Si equilibrium concentration of 0.4 mg l^{-1} for EVPT[MJJASO] = 85% (Case 1, Section 'The Si balance of Lake SHL'), $Si_{(initial)}$ = 0 mg l^{-1}, $Si_{(rain)}$ = 0.07 mg l^{-1}, $Si_{(GW)}$ = 12.5 mg l^{-1}. (b) Same conditions as in (a), but diffusive reflux of dissolved Si from the surface sediments considered (Case 2). (c) Same conditions as in (b), but percolation of half of winter precipitation considered (Case 3). (d) Hydrological conditions as for cases 1 and 2, but diffusive reflux of Si from the surface sediments as the only Si-source considered. Note that Si_{equ} is only less influenced by the water budget of the lake for such a parameter setting.

were derived by modelling the condition of Si_{equ} = 0.4 mg l^{-1}. Inflow of Si-rich groundwater was assumed to be uniform at all depth sections. The bio-availability of dissolved Si in the dimictic lake may theoretically reach a value of ca. 0.72 for complete Si-consumption in the upper 15 m of the water column. Estimates of the biogenic uptake of dissolved Si which fit Si_{equ} = 0.4 mg l^{-1} account for about half of this value (see above). The relative biogenic uptake of dissolved Si derived from the inflow of groundwater could be distinctly higher, if a major proportion of the groundwater discharged into depth section I of the lake basin. Dilution by rainfall onto the lake surface camouflages the inflow of mineralised groundwater into the epilimnion during the rainy season. However, groundwater discharge into the epilimnion is clearly documented in Si water-profiles from September and October (Figure 4).

In our mass balance model, complete biogenic uptake of the external Si input accounts for F_{focus} = 3.69 to achieve a net-accumulation of biogenic silica of 17 g m^{-2} yr^{-1} at the centre of the lake bottom (Si_{equ} = 0.4 mg l^{-1}, parameter

setting as in Case 2 , Figure 20b). The solid lines, shown in Figure 21, give the balanced values of F_{uptake} (numbers above the lines) that fit Si_{equ} = 0.4 mg l^{-1} for various values of EVPT and hypothetical portions (numbers along the lines) of the external Si input that get completely transferred to diatomaceous matter, which give a net flux of biogenic silica of 17 g m^{-2} yr^{-1} at the centre of the lake bottom for EVPT[MJJASO] = 85%. The considered flux of biogenic silica (17 g m^{-2} yr^{-1}) represents the lower limit for the sedimentation period between 1830 and 1947, which might be representative for dry periods. The real net accumulation of biogenic silica might be overestimated by ca. 10% of this value for analytical reasons. Considering 15.3 g m^{-2} yr^{-1} as a lower limit for the net accumulation of biogenic silica decreases the necessary focussing factor only insignificantly from 4.79 to 4.4 to obtain Si_{equ} of the modern mixed lake (model case shown in Figure 21).

Percolation of winter precipitation. Mean atmospheric temperatures between November and March are below zero in the region. Seepage of precipitation is not possible as long as the topsoil is frozen. There may be relatively short periods in late autumn and spring during which formation of groundwater may be favoured due to reduced transpiration of the woody vegetation. The dashed line in Figure 21 demonstrates the correlation between F_{uptake} and EVPT that would be achieved if half of mean winter precipitation were considered as additional groundwater discharge with 12.5 mg l^{-1} dissolved Si. The related value of F_{focus} which gives F-$bSiO_2^{total}$ = 17 g m^{-2} yr^{-1} for the flat lake bottom is 3.15.

Mean annual precipitation. Data on precipitation for the periods May–October (661 mm) and November–April (114 mm), respectively, represent mean values for the period 1955–1997 measured at the nearby meteorological station of Jingyu. Precipitation during the summer monsoon shows a relative standard deviation of 22% in this period (Table 2). Lake Sihailongwan (797 m a.s.l.) is 248 m above the city of Jingyu (549 m a.s.l.) and it is likely that mean local precipitation is higher than that in Jingyu. Figure 22 shows the correlation between EVPT and F_{uptake} for 20% higher and lower precipitation during the summer and winter monsoon (parameter setting as Case 2, Section 'Biogenic uptake of Si', but 50% complete biogenic uptake of the external Si input assumed). Related variations

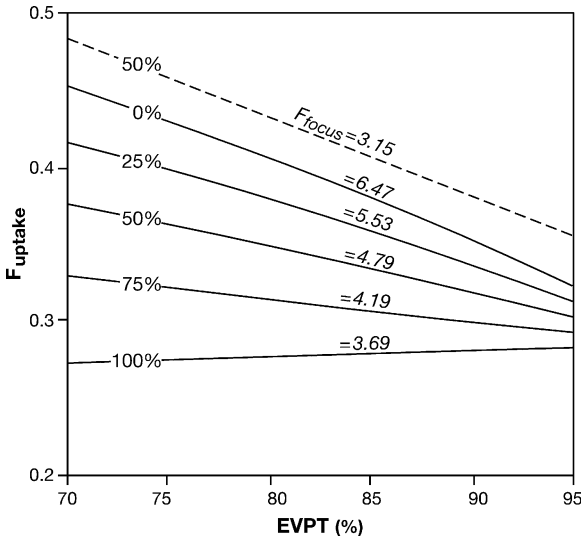

Figure 21. Biogenic uptake-rates for dissolved Si (F_{uptake}) which fit the Si equilibrium concentration of the modern mixed-lake for various values of EVPT (*x*-axis) and various proportions of complete uptake of the external Si input (numbers above the lines). Setting of hydrological parameters as in Figures 5a and 20a, b. *Solid lines*: No percolation of winter precipitation. *Dashed line*: Percolation of half of winter precipitation. *Italic numbers*: Necessary focussing of sediment accumulation (F_{focus}) that gives a F-$bSiO_2$ value of 17 g m^{-2} yr^{-1} at the flat lake bottom for EVPT = 85%.

for the balanced values of F_{uptake} and F_{focus} are only minor for such changes in the hydrological conditions. The necessary focussing of sediment accumulation to obtain F-$bSiO_2$ of 17.0 g m^{-2} yr^{-1} declines from 4.79 to 4.18 for 20% higher precipitation and EVPT = 85%.

Groundwater discharge close to the lake margin was sampled during the summer monsoon in 1999 and 2001. Measured Si concentrations deviate less than 5% from the mean value of 12.5 mg l^{-1}. The acidification trend in the catchment may have affected silicate weathering and the mobility of chemical elements released by silicate weathering. The leaching of phosphorus may have increased due to the lowering of the pH in percolating fluids, whereas the mobility of Si should have decreased. The dissolved Si concentration in the groundwater discharge may have been higher, and the influx of SRP (soluble reactive phosphorus) lower during former periods. Distinctly higher production of diatomaceous matter during former periods would be unlikely if diatom production was generally limited by SRP-availability. The Si_{equ} concentration of the lake is adjusted within a relatively short

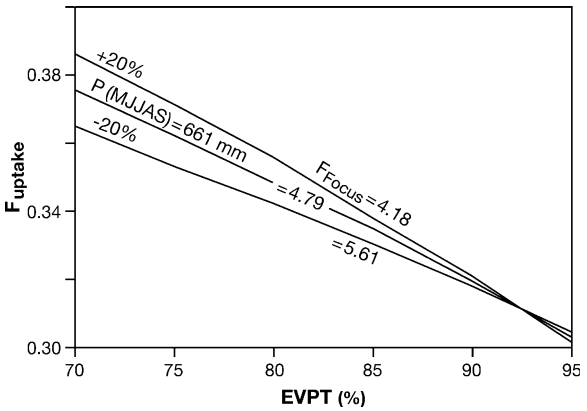

Figure 22. Balanced biogenic up-take of dissolved silica that fits Si_{equ} = 0.4 mg l^{-1} – dependence on EVPT for 20% higher and 20% lower precipitation, respectively. Necessary focussing of sediment accumulation towards the flat lake bottom decreases from 4.79 to 4.18 for 20% higher precipitation. Hydrological conditions as in Figure 20b, 50% complete uptake of F-$bSiO_2$(ext) considered.

period of ca. 5 years (Figure 20). It may have been higher for lower SRP concentrations in the groundwater discharge. Figure 23 shows the correlation between EVPT and F_{uptake} for various values of Si_{equ} (0.4, 0.5, 0.6 mg l^{-1} Si). Such a variation in the parameter setting also only slightly influences the balanced values of F_{focus} which are necessary to get F-$bSiO_2{}^{total}$ = 17 g m^{-2} yr^{-1} at the flat lake bottom.

Synopsis

Based on bulk chemical data of the annually laminated SHL sediment record, the balance between dust influx by dry- and wet-deposition and the Al_2O_3 concentrations of the related dust components could be estimated by combined geochemical mass balances for a probable variation range of F-$bSiO_2{}^{int}$. We use a Si-balance model of the lake, based on hydrochemical monitoring data, to get a closer estimate of F-$bSiO_2{}^{int}$, and independent estimates for the net accumulation of biogenic silica at the flat lake bottom. In our model, a net flux of biogenic silica related to internal forcing can be only obtained for the flat lake bottom if focussing of the particle flux towards the centre of the lake basin exists. For a wet and dry sedimentation interval, we exemplarily calculate the focussing of the particle flux, which is necessary to achieve correspondence between the two independent estimates of F-$bSiO_2{}^{total}$, in the following.

The minimum flux of biogenic silica at the flat lake bottom (F-$bSiO_2{}^{total}$ = 17 g m^{-2} yr^{-1}, corrected for Si-leaching from siliciclastics) is obtained for sample 10, which represents sedimentation for a dry period around 1930 (Figure 8). Figure 24a shows the proportion of F-$bSiO_2{}^{int}$ in the total net accumulation of biogenic silica at the flat lake bottom for variable values of EVPT, P[MJJASO] = 661 mm, assumed 50% complete uptake of the Si influx via groundwater inflow and 20% lower and higher annual precipitation, respectively (see Figure 22). The numbers above the lines give the necessary value of F_{focus} to obtain F-$bSiO_2{}^{total}$ = 17 g m^{-2} yr^{-1} for EVPT[MJJASO] = 85%. The shown F-$bSiO_2{}^{int}$/F-$bSiO_2{}^{total}$ values plot within a small variation range for 20% higher and lower precipitation. The balanced value of F-$bSiO_2{}^{int}$ for EVPT[MJJASO] = 85% and 20% higher annual precipitation is 4.5 g m^{-2} yr^{-1} and accounts for ca. 30% of F-$bSiO_2{}^{total}$. The derived value for F-$bSiO_2{}^{int}$ falls in the probable variation range of F-$bSiO_2{}^{int}$ elucidated by mass balances based on chemical sediment composition and corresponds with a flux rate of 54 g m^{-2} yr^{-1} for the input of dust by drydeposition (F-All^{dry}). The related Al_2O_3 concentration of the dry deposited dust fraction ($Al_2O_3[All^{dry}]$) is 13.4 wt.% (see Figure 18, Tables 5 and 6).

Sample 15 represents sedimentation for relative enhanced rainfall during the summer monsoon around 1866 (wet period). The mean total net accumulation of biogenic silica is 27 g m^{-2} yr^{-1} for the sedimentation interval represented by this sample. The necessary sediment focussing to obtain F-$bSiO_2{}^{total}$ is balanced similarly to the above estimate for EVPT[MJJASO] = 85%, but we consider 1.5 times higher annual precipitation. F-$bSiO_2{}^{total}$ = 27 g m^{-2} yr^{-1} can be balanced for F_{focus} = 5.18 which gives a value of 6.1 g m^{-2} yr^{-1} for F-$bSiO_2{}^{int}$. The slightly higher value for F-$bSiO_2{}^{int}$ accounts for a dust influx by drydeposition of 62 g m^{-2} yr^{-1} and an Al_2O_3 concentration of 14.3 wt.% for the dry deposited dust fraction.

The derived individual estimates of F_{focus}, F-$bSiO_2{}^{int}$, and F-All^{dry} for a dry and a wet period do not much differ from each other. Influx of dust by dry-deposition is relatively constant and F-All^{wet}/F-All^{dry} clearly enhanced for wet periods. The balanced values for F-$bSiO_2{}^{int}$ fall in a close

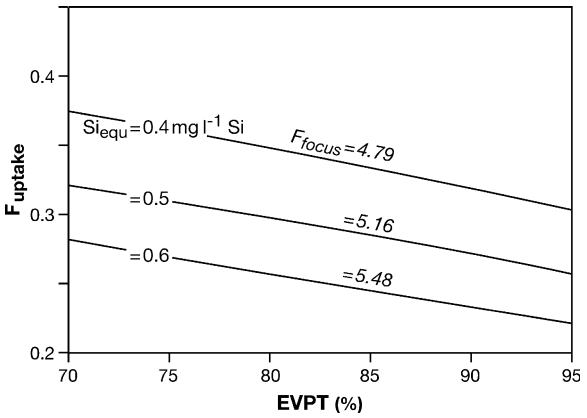

Figure 23. Balanced biogenic up-take of dissolved silica for various hypothetical values of Si_{equ}, dependence on EVPT. Hydrological setting as in Figure 20a and b; 50% complete uptake of the external Si-influx. *Italic numbers*: Necessary sediment focussing (F_{focus}) to give F-$bSiO_2$ = 17 g m^{-2} yr^{-1} at the centre of the lake bottom for EVPT = 85%.

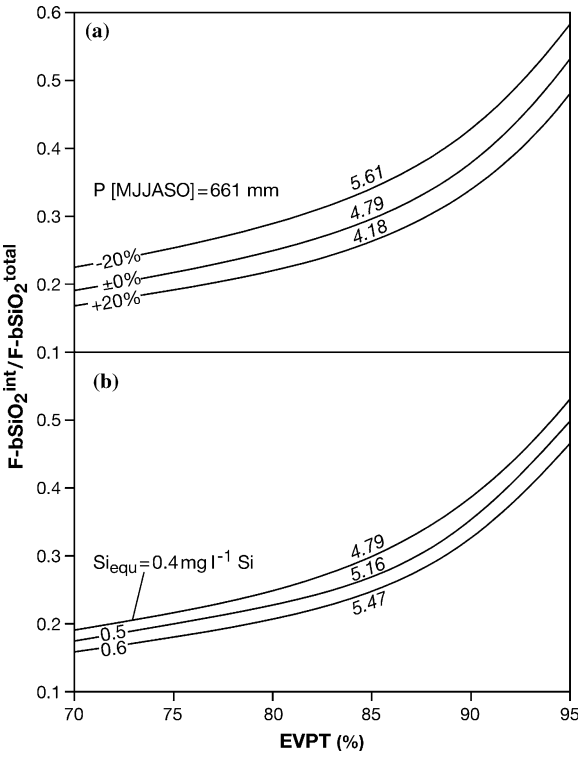

Figure 24. (a) Balanced proportions of internal forced net accumulation of biogenic silica (F-$bSiO_2^{int}$) in the total net flux of biogenic silica (F-$bSiO_2^{total}$) at the flat lake bottom for parameter settings as in Figure 22 – dependence on precipitation and EVPT. (b) Balanced proportions of internal forced net accumulation of biogenic silica (F-$bSiO_2^{int}$) in the total net flux of biogenic silica (F-$bSiO_2^{total}$) at the flat lake bottom for parameter settings as in Figure 5, dependence on Si_{equ} and EVPT.

variation range (ca. 5–6 g m^{-2} yr^{-1}). This allows a closer estimate of F-All^{dry} (ca. 55–60 g m^{-2} yr^{-1}) and of the Al_2O_3 content of the dry deposited dust fraction (ca. 14 wt.%) than it would be possible by geochemical mass balances based on sediment composition alone. For F_{focus} = 5, which gives correspondence between the independent estimates of F-$bSiO_2^{total}$, sediment accumulation in the depth sections I and II is by 54% reduced.

The total dust flux by dry- and wet-deposition onto the surface of Lake SHL between 1830 and 1970 varies between 16 and 28 g m^{-2} yr^{-1} with a mean value of 22 g m^{-2} yr^{-1}. These estimates are based on the F-Al_2O_3 values given in Table 2. We consider for these estimates a Al_2O_3 content of 17.5% for the bulk siliciclastic sediment fraction (All^{total}), 25% contribution by in-wash of local soil particles, and F_{focus} = 5. The F-All^{wet}/F-All^{dry}

Table 6. Synthesised compilation of geochemical mass balance results.

P[775]·x (mm yr^{-1})	F-$bSiO_2^{total}$ (g m^{-2} yr^{-1})	F-$bSiO_2^{int}$/ F-$bSiO_2^{ext}$	F-$bSiO_2^{int}$ (g m^{-2} yr^{-1})	F-All^{dry} (g m^{-2} yr^{-1})	F_{focus}	$Al_2O_3(All^{dry})$ (wt.%)	F-All^{wet}/F-All^{dry} m. (Sampl.): 9–17
Dry period			EVPT[MJJASO] = 85%				
x = 0.8	17	0.34	5.9	58.6	5.61	14.5	1.6
x = 1.0	17	0.30	5.1	54.1	4.79	14.1	1.8
x = 1.2	17	0.26	4.5	50.8	4.18	13.8	2.0
Wet period							
x = 1.5	27	0.22	6.1	57.7	5.18	14.6	
Sample	SR_m (g m^{-2} yr^{-1})	F-Au^{total} (g m^{-2} yr^{-1})	F-$bSiO_2^{total}$ (g m^{-2} yr^{-1})	F-$bSiO_2^{int}$ (g m^{-2} yr^{-1})	F_{focus}	$Al_2O_3[All^{dry}]$ (wt.%)	$Al_2O_3[All^{wet}]$ (wt.%)
10	171.7	38.5	17.5	4.5	4.18	13.8	18.9
15	238.1	60.3	27.4	6.1	5.18	14.6	19.8

ratio of the individual sediment samples 9–17 (sedimentation interval: 1830–1947) varies between 1.0 and 2.0 for F-$bSiO_2^{int}$ = 6 g m^{-2} yr^{-1} and is 1.6 at its mean (Table 5). The focussing of the particle-flux towards the flat lake bottom might be higher for clay-sized particles and 'light' organic seston than for silt-sized mineral grains that probably represent the major portion of the aeolian influx by dry deposition. The derived values for F-All^{wet}/F-All^{dry} characterise the depositional flux at the flat lake bottom. They may therefore tentatively overestimate the real contributions by wet-deposition of dust onto the surface of the lake.

Enhanced fall-out of mineral particles related to dust storms, has been historically recorded over extensive areas of north-eastern and south-eastern China (e.g., Zhang 1984 and Zhang et al. 1997). The peak in dust reports is from late April to early May (Merrill et al. 1989, and references therein). Measurements of the monthly dust fall-out along a west-east transect from the Hexi-Corridor to the western loess Plateau (see Figure 1) carried out in the period 1988–1991 (Derbyshire et al. 1998) documented a minimum in the dust flux in November and December. The winter minimum is explained by seasonal freezing of the ground in the source regions of the dust. There were further peaks in dust deposition in summer and in autumn. In general, the deposition of dust remained substantial until late autumn.

Mineral aerosols can be transported at higher atmospheric levels by the zonal westerlies towards the western Pacific (e.g., Prospero et al. 1989). The prevailing of strong northwesterlies during the winter monsoon in East Asia favours the near surface transport of dust towards the East China Sea particular during winter (Figure 1a). Estimates of the annual atmospheric dust flux for the East China Sea (see Figure 1) based on coastal and off-shore sampling sites range between 5 and 100 g m^{-2} yr^{-1} (monitoring period: December 1990 to June 1993, Gao et al. 1997), with the mean value of 27 g m^{-2} yr^{-1}. In spring, mean monthly dust deposition by dry-deposition (1.3 g m^{-2} $month^{-1}$) and dust flux by wet-deposition (1.3 g m^{-2} $month^{-1}$) reached a similar order of magnitude. Holocene dust flux rates, reconstructed from various North-west Pacific marine sediment records, approximately 2500 km off the Chinese mainland (see Figure 1a for core locations), show a latitudinal dependence. They vary between 5 and 15 g m^{-2} yr^{-1} with a maximum at around 38° N (Rea and Leinen 1988).

Our study documents that mean annual dust flux in the Long Gang area for the period between 1830 and 1947 is similar to estimates for mean annual dust flux rates for the Yellow and East China Sea that are based on modern dust trap measurements. Total deposition of dust in the Long Gang area during the rainy season reaches the same order of magnitude and can even exceed the dust flux during the winter monsoon. Decadal variations in the annual dust flux largely reflect variations in the dust deposition during the summer monsoon by wet-deposition. The inferred positive correlation between rainfall and dust flux during the summer monsoon implies that dust deposition is determined by the out-wash efficiency of mineral particles for a permanent high atmospheric dust content over Northeast China. Mean annual dust flux over Northeast China, as estimated in this study, exceeds dust flux estimates by Rea and Leinen (1988) for the NW Pacific, ca. 2500 km east off the Long Gang area about 2.5 times. A decline in dust deposition rates in this order of magnitude might be typical for the long-range transport of atmospheric mineral aerosols at higher atmospheric levels.

Acknowledgements

We thank Prof. Liu Jiaqi and his co-workers Chu Guoqiang and Ni Yunyan for their help in organising the field campaigns, D. Berger, M. Köhler for assistance with coring, and U. Kegel, St. Flechsig, Chr. Wiesenberg, and Chr. Adler for technical support in the GFZ-laboratories. Dr P. Dulski is thanked for ICP-MS measurements, and Dr Gottschalk and Mrs Bauer for carrying out quantitative XRD-analyses. We are grateful to A. Hendrich for his support in preparing the numerous figures, and to Dr A. Lücke and Dr B. Mingram for stable isotope measurements of the water samples. We highly appreciate the substantial editorial effort by Prof. W.M. Last and Dr J. Holmes and their help to improve the initial MS. Prof. R. Hetzel is thanked for subsampling of 4 loess profiles in the Hexi-Corridor and Prof. J. Sun for making original data on geochemical loess composition available. The investigations were financed by the GFZ-Potsdam as part of the German-Chinese Science co-operation.

Appendix A. List of abbreviations

All, All^{total}	Total (allochthonous) siliciclastic sediment fraction
Au, Au^{total}	Total autochthonous sediment fraction including organic matter and biogenic silica. The extension 'total' is used in the text, if various Au and All-components are discriminated. Estimates for Au and All are based on the following considerations: The sum of Au and All accounts for values distinct above 100 wt.%, if we consider (i) 10 wt.% water content of the biogenic opal and '2.13·TOC' as an estimate for the organic matter concentration (Dean 1974), and (ii) mean continental crust composition for All (Al_2O_3 = 15.6 wt.%, Taylor 1964). 'Au + All' values < 100 wt.% could be obtained, if an Al_2O_3 concentration of 19.35 wt.% was assumed for All. Such a high Al_2O_3 concentration does not correspond with the mineralogical composition of the SHL-sediments. Au would account for the sum of TOC and $bSiO_2$ only if an Al_2O_3 concentration of 15.6 wt.% was assumed for All. We consider an Al_2O_3 concentration of 17.5 wt.% for All and '1.1·$bSiO_2$ + 1.8·TOC' for Au. This gives 'Au + All' values < 100 wt.% for all sediment samples. Since the $bSiO_2$/TOC ratio is rather constant for sediments below 9 cm we alternatively calculate the concentration of Au by '2.2 $bSiO_2$' for sediments below 9 cm and by '2.5 · $bSiO_2$' for sediments above 9 cm throughout in the manuscript
All^{wet}	The portion of the siliciclastic input which is positively correlated with rainfall during the summer monsoon. It largely originates from aeolian influx by wet-deposition and is called wet deposited dust fraction in the manuscript for simplification
All^{dry}	The portion of the siliciclastic input which is not correlated with the summer monsoon strength. It largely represents aeolian influx by dry deposition and is called dry deposited dust fraction in the manuscript for simplification
$Al_2O_3[All^{dry}]$	Al_2O_3 content of the dry deposited dust fraction
$Al_2O_3[All^{wet}]$	Al_2O_3 content of the wet deposited dust fraction
Au^{int}	Portion of the total autochthonous sediment constituent at the flat lake bottom (Au^{total}) which is related to lake-internal forcing of bioproduction
$bSiO_2$	Biogenic silica (concentration values given in SiO_2)
Eu_N/Eu_N^*	Europium anomaly for PAAS-normalized REE-concentrations calculated by $Eu_N/(0.5 \cdot Nd_N + 0.5 \cdot Tb_N)$ in the manuscript
F-All, $F\text{-}All^{total}$	Annual siliciclastic deposition rate obtained at the flat lake bottom
$F\text{-}All^{wet}$	Siliciclastic deposition rate at the flat lake bottom originating from aeolian influx by wet deposition
$F\text{-}All^{dry}$	Siliciclastic deposition rate at the flat lake bottom originating from aeolian deposition by dry deposition
F-Au, $F\text{-}Au^{total}$	Annual net accumulation rate of Au^{total} for sediments from the flat lake bottom
$F\text{-}Au^{int}$, $F\text{-}Au^{int}$	Annual net accumulation of autochthonous sediment constituents at the flat lake bottom controlled through lake internal forcing
$F\text{-}bSiO_2$	Flux of biogenic silica expressed in mass units SiO_2. It means the net accumulation rate of biogenic silica at the flat lake bottom if not specified otherwise in the text
$F\text{-}bSiO_2^{int}$	The portion of $F\text{-}bSiO_2$ which is controlled by lake internal forcing. Estimates for $F\text{-}bSiO_2^{int}$ are derived by modelling based on the Si-budget of Lake SHL. It represents the diffusive Si reflux from the surface sediments of the whole lake basin which gets seasonally transferred into diatomaceous matter and gives a net accumulation of $bSiO_2$ at the flat bottom of the U-shaped lake basin by sediment focussing. F- $bSiO_2^{int}$ values above 0 could not be obtained without focussing of the particle flux towards the centre of the lake for our model assumptions
$F\text{-}bSiO_2^{corr}$	Estimates the portion of $F\text{-}bSiO_2^{total}$ which is controlled by external forcing
$F\text{-}bSiO_2^{total}$	Annual net accumulation of $bSiO_2$ obtained at the flat lake bottom meaning the same as $F\text{-}bSiO_2$. The extension 'total' is used when individual contributions by external and internal forcing are discussed in the text
F-TOC	Annual net accumulation of TOC obtained at the flat lake bottom
HREE	Heavy Rare Earth Element
IC	Inorganic carbon
La_N/Yb_N	PAAS-normalized REE-ratio
N_v	Number of varves per individual sample slice or per cm as specified in the text
PAAS	Post Archean Australian Shale. REE-concentrations for mean PAAS composition after Taylor and McLennan (1985) are used for REE-normalization in the manuscript
Φ (0…1)	Porosity
ρ_s (g cm^{-3})	Density of the solid sediment
REE	Rare Earth Element

SR_m (g m^{-2} yr^{-1})	Mean annual mass accumulation rates for the periods represented by the individual sediment sample slices: $SR_m = (1 - \Phi)\cdot\rho_s\cdot 10000/N_v$
SR_m^{exc}	SR_m excess various other flux variables, used in a general sense
SR_m^{corr1}	Mean annual mass accumulation minus internal forced flux of biogenic matter (F-Au^{int})
SR_m^{corr2}	Mean annual mass accumulation minus internal forced flux of biogenic matter (F-Au^{int}) minus dust influx by dry deposition (F-All^{dry})
TOC	Total organic carbon
W_c (wt.%)	Water content determined by weight difference before and after freeze-drying
Specific terms used in the Si-balance model of Lake SHL	
$A_{Basin}^{0–15\ m}$	Surface of the lake basin for the given depth sections based on detailed depth measurements during the field campaign in 2001
$A_{Catchment}$	Size of the hydrological catchment. We assume that it corresponds with the interior of the SHL-crater
$A_{Lake}^{Surface}$	Surface of the lake
EVP_{Lake}	Annual evaporation rate for the lake surface
EVPT	Evapotranspiration
$EVPT_{Catchment}$[MJJASO]	EVPT in percent of precipitation for the period given in brackets
F-	Symbol generally used for flux rates
F-$SiO_{2(refl)}$	Diffusive reflux from the surface sediments, assumed to be constant for the whole lake basin, and estimated by the First Fick's law for a Si concentration gradient obtained in a similar maar lake
F-$SiO_{2(inflow)}$	Annual dissolved Si influx by inflow of groundwater
F-$SiO_{2(outflow)}$	Annual lost of Si by subsurface outflow
F-$SiO_{2(dep)}$	The depositional flux of biogenic silica
F_{focus}	Ratio between real sediment accumulation at the flat lake bottom and the hypothetical sediment accumulation for the whole lake basin if no sediment focussing is present
F_{uptake} (0…1)	Factor that describes the biogenic uptake of dissolved Si
$Inflow_{(Surface)}$	Annual surface run-off from the catchment. Surface run-off is assumed to have negligible dissolved Si-concentrations
$Inflow_{(GW)}$	Annual groundwater discharge from the catchment. Groundwater inflow is assumed to have 12.5 mg l^{-1} dissolved Si
P	Annual precipitation rate
P[MJJASO]	Total amount of precipitation for the period given in brackets
Outflow	Annual subsurface outflow of the lake resulting from the setting of hydrological parameters
Si^{accum}	Lake-water dissolved Si which gets seasonally accumulated in the deep water during the stagnation periods
Si_{equ}	Dissolved Si concentration for the mixed lake at steady state. We assume that the Si concentration of the modern mixed-lake is close to steady state; Si_{equ} is adjusted by inflow of Si-rich groundwater, rainfall on to the lake surface surface run-off, subsurface outflow, biogenic Si-uptake and diffusive Si reflux from the surface sediments. Since dissolved lake water concentrations are low and diatom production is not strongly limited by P-availability, annual biogenic uptake accounts for nearly 50% of the dissolved Si-inventory of the lake; Si_{equ}, therefore adjusts within only few years though water residence time of Lake SHL is rather high (ca. 36 yrs). Equilibrium concentrations of Na and Mg (Na_{equ}, Mg_{equ}) are less affected by bio-production, their adjusting therefore needs much longer
SRP	Soluble reactive phosphorus
$V_{Lake}^{0–15\ m}$	Water volume for the given depth section

References

Araguás-Araguás L., Froehlich K. and Rozanski K. 1998. Stable isotope composition of precipitation over southeast Asia. J. Geophys. Res. 103, D22: 28,721–28,742.

Araguás-Araguás L., Froehlich K. and Rozanski K. 2000. Deuterium and oxygen-18 composition of precipitation and atmospheric moisture. Hydrol. Process. 14: 1341–1355.

Chu G., Liu J., Schettler G., Li J., Sun Q., Gi Z., Lu H., Liu Q. and Liu T. 2005. Sediment fluxes and varve formation in Sihailongwan, a maar lake of northeastern China. J. Palaelimnol. 34: 311–324.

Dean W.E. 1974. Determination of carbonate and organic matter in calcareous sediments and sedimentary rocks by loss on ignition: comparison with other methods. J. Sediment. Petrol. 44: 242–248.

Derbyshire E., Meng X. and Kemp R.A. 1998. J. Arid Environ. 39: 497–516.

Ding Z.L., Sun J.M., Yang S.L. and Liu T.S. 2001. Geochemistry of the Pliocene red clay formation in the Chinese Loess Plateau and implications for its origin, source provenance and paleoclimate change. Geochim. Cosmochim. Acta 65: 901–913.

Domrös M. and Peng G. 1988. The Climate of China. Springer, Heidelberg, 360 pp.

Dulski P. 2001. Reference materials for geochemical studies: new analytical data by ICP-MS and critical discussion of reference values. Geostandard. Newslett. 25: 87–125.

Gao Y., Arimoto R., Duce R.A., Zhang X.Y., Zhang G.Y., An Z.S., Chen L.Q., Zhou M.Y. and Gu D.Y. 1997. Temporal and spatial distributions of dust and its deposition to the China Sea. Tellus 49: 72–189.

GNIP (Global Network of Isotopes in Precipitation) database: http://isohis.iaea.org/GTNIP.asp

Gonfiantini R. 1986. Environmental isotopes in lake studies. In: Fritz P. and Fontes J.Ch. (eds), Handbook of Environmental Isotope Geochemistry, Vol. 2, The Terrestrial Environment B. Elsevier, Amsterdam, pp. 113–168.

Hu Z.-Z. 1997. Interdecadal variability of summer climate over East Asia and its association with 500 hPa height and global sea surface temperature. J. Geophys. Res. 102, D16: 19,403–19,412.

Hurley J.P., Armstrong D.E., Kenoyer G.J. and Bowser C.J. 1985. Ground water as a silica source for diatom production in a precipitation-dominated lake. Science 227: 1576–1578.

Klee R. and Schmidt R. 1987. Eutrophication of Mondsee (Upper Austria) as indicated by the diatom stratigraphy of a sediment core. Diatom Res. 2: 55–76.

Larson A.C. and Von Dreele R.B. 1987. Generalized structure analysis system. Los Alamos National Laboratory Report No. LA-UR-86-748, 224 pp.

Merril J.T., Uematsu M. and Bleck R. 1989. Meteorological analysis of long range transport of mineral aerosols over the North Pacific. J. Geophys. Res. 94, D6: 8584–8598.

Mingram J., Allen J.R.M., Brüchmann C., Liu J., Luo J., Negendank J.F.W., Nowaczyk N. and Schettler G. 2004. Maar- and crater lakes of the Long Gang Volcanic Field (N.E. China) – overview, laminated sediments, and vegetation history of the last 900 years. Quatern. Int. 123–125: 35–147.

Prospero J.M., Uematsu M. and Savoie D.L. 1989. In: Riley J.P., Chester R. and Duce R.A. (eds), Dust transport to the Pacific Ocean. Chemical Oceanography 10, Academic Press, San Diego, CA, pp. 188–218.

Rea D.K. and Leinen M. 1988. Asian aridity and the zonal westerlies: Late Pleistocene and Holocene record of eolian deposition in the northwest Pacific ocean. Palaeogeogr. Palaeoclimatol. Palaeoecol. 66: 1–8.

Schettler G., Mingram J., Negendank J.F.W. and Liu J. 2006. Palaeovariations in the East-Asian Monsoon regime geochemically recorded in varved sediments of Lake Sihailongwan (Northeast China, Jilin province). Part 2: A 200 year record of atmospheric lead-210 flux variations and its palaeoclimatic implications. J. Paleolimnol 35: 271–288.

Sun J. 2002. Provenance of loess material and formation of loess deposits on the Chinese Loess Plateau. Earth Planet. Sci. Lett. 203: 845–859.

Taylor S.R. 1964. The abundance of chemical elements in the continental crust – a new table. Geochim. Cosmochim. Acta 28: 1273–1285.

Taylor S.R. and McLennan S.M 1985. The Continental Crust: Its Composition and Evolution. Oxford, Blackwell, 312 pp.

Warnecke G. 1991. Meterologie und Umwelt. Springer, 342 pp.

Wei K. and Gasse F. 1999. Oxygen isotopes in lacustrine carbonates of West China revisited: implications for post glacial changes in summer monsoon circulation. Quatern. Sci. Rev. 18: 1315–1334.

Wilcox E.M. and Ramanathan V. 2004. The impact of observed precipitation upon the transport of aerosols from South Asia. Tellus 56: 35–450.

Wu Z. 1980. Vegetation of China. Science Press (in Chinese), Beijing, 1382 pp.

Xiao J., Inouchi Y., Kumai H., Yoshikawa S., Kondo Y., Liu T. and An Z. 1997. Eolian quartz flux to Lake Biwa, Central Japan, over the past 145,000 years. Quatern. Res. 48: 48–57.

Zhang D.E. 1984. Synoptic-climatic studies of dust fall in China since the historic times. Sci. Sin. 27: 825–836.

Zhang X.Y., Arimoto R. and An Z.S. 1997. Dust emission from Chinese sources linked to variations in atmospheric circulation. J. Geophys. Res. 102, D23: 28,041–28,047.